

Ca II Triplet Spectroscopy of Small Magellanic Cloud Red Giants. I. Abundances and Velocities for a Sample of Clusters

M.C. Parisi

Observatorio Astronómico, Universidad Nacional de Córdoba
Laprida 854, Córdoba, CP 5000, Argentina.

`celeste@oac.uncor.edu`

A.J. Grocholski

Space Telescope Science Institute
3700 San Martin Dr., Baltimore, MD 21218, USA.

`aarong@stsci.edu`

D. Geisler

Departamento de Astronomía, Universidad de Concepción
Casilla 160-C, Concepción, CP 4030000, Chile

`dgeisler@astro-udec.cl`

A. Sarajedini

Department of Astronomy, University of Florida
PO Box 112055, Gainesville, FL 32611, USA.

`ata@astro.ufl.edu`

and

J.J. Clariá

Observatorio Astronómico, Universidad Nacional de Córdoba
Laprida 854, Córdoba, CP 5000, Argentina.

claria@oac.uncor.edu

Received _____; accepted _____

ABSTRACT

We have obtained near-infrared spectra covering the Ca II triplet lines for a large number of stars associated with 16 SMC clusters using the VLT + FORS2. These data compose the largest available sample of SMC clusters with spectroscopically derived abundances and velocities. Our clusters span a wide range of ages and provide good areal coverage of the galaxy. Cluster members are selected using a combination of their positions relative to the cluster center as well as their location in the CMD, abundances and radial velocities. We determine mean cluster velocities to typically 2.7 km s^{-1} and metallicities to 0.05 dex (random errors), from an average of 6.4 members per cluster. By combining our clusters with previously published results, we compile a sample of 25 clusters on a homogenous metallicity scale and with relatively small metallicity errors, and thereby investigate the metallicity distribution, metallicity gradient and age-metallicity relation (AMR) of the SMC cluster system. For all 25 clusters in our expanded sample, the mean metallicity $[\text{Fe}/\text{H}] = -0.96$ with $\sigma = 0.19$. The metallicity distribution may possibly be bimodal, with peaks at ~ -0.9 dex and -1.15 dex. Similar to the LMC, the SMC cluster system gives no indication of a radial metallicity gradient. However, intermediate-age SMC clusters are both significantly more metal-poor and have a larger metallicity spread than their LMC counterparts. Our AMR shows evidence for 3 phases: a very early (> 11 Gyr) phase in which the metallicity reached ~ -1.2 dex, a long intermediate phase from $\sim 10 - 3$ Gyr in which the metallicity only slightly increased, and a final phase from 3–1 Gyr ago in which the rate of enrichment was substantially faster. We find good overall agreement with the model of Pagel & Tautvaišienė (1998), which assumes a burst of star formation at 4 Gyr. Finally, we find that the mean radial velocity of the cluster system is 148 km s^{-1} , with a velocity dispersion of 23.6 km s^{-1} and

no obvious signs of rotation amongst the clusters. Our result is similar to what has been found from a wide variety of kinematic tracers in the SMC, and shows that the SMC is best represented as a pressure supported system.

Subject headings: galaxies: star clusters — Magellanic Clouds — stars:abundances

1. Introduction

The Small Magellanic Cloud (SMC) has long been recognized as being of fundamental importance for a wide variety of astrophysical studies. First, the current paradigm of galaxy formation suggests that spiral galaxy spheroids, such as the Milky Way (MW) halo, are formed by the accretion/merger of smaller, satellite galaxies (e.g., Searle & Zinn 1978; Zentner & Bullock 2003). As one of the nearest low mass galaxies known, the SMC is thus a possible prototype of pre-Galactic fragments. However, current Λ CDM models suggest that the majority of the MWs building blocks were assimilated very early in its history and that existing low mass galaxies like the SMC are survivors of this process and thus underwent a different chemical evolution (e.g., Robertson et al. 2005). At the least, many dynamical simulations (e.g., Bekki et al. 2004) suggest that the MW, Large Magellanic Cloud (LMC) and SMC compose a longterm interacting system, with the SMC and LMC likely to be eventually consumed by the MW. In addition, close encounters in the last few Gyr may well have stimulated star formation on a global scale in both the SMC and LMC (Murai & Fujimoto 1980; Gardiner et al. 1994; Yoshizawa & Noguchi 2003; Bekki et al. 2004). These early simulations predict bursts of star formation ~ 0.2 Gyr ago that led to the formation of the eastern wing of the SMC and the Magellanic Bridge, and a similar close encounter event some 4 Gyr ago. Note however that the accurate proper motions crucial for properly modeling the orbits of the SMC and LMC are still problematic, and that the most recent values all suggest the Magellanic Cloud may be unbound to each other and only beginning their first close encounter with the MW (Kallivayalil et al. 2006; Piatek et al. 2008). The SMC, with its low global metallicity, is the best local counterpart to the host of distant dwarf irregular and blue compact dwarf galaxies, making it an attractive target for exploring the importance of metallicity in a number of contexts, including star formation, initial mass function, stellar and galaxy evolution, etc.

In particular, the star clusters of the SMC, because they are (at least to first order) simple stellar populations (SSPs), are an invaluable resource with which we can explore the structure, kinematics, star formation and chemical evolution history of the SMC. As a majority of stars may have formed in clusters (see e.g., Lada & Lada 2003 for the solar neighborhood and Chandar et al. 2006 for the SMC, but see Bastian et al. 2009 for an opposing view), their study has become even more relevant. On a cosmological scale, star clusters in the SMC are of utmost importance for the study and understanding of stellar populations in distant galaxies, since they cover age and abundance space that is not occupied by their Galactic counterparts. In addition, while the LMC cluster system suffers from the well known age gap, where only one cluster is known to have formed between ~ 3 and ~ 13 Gyr ago, (i.e. during 3/4 of its life; Da Costa 1991, Geisler et al. 1997), the SMC possesses clusters that have been forming more or less continuously over the past ~ 11 Gyr (e.g., Glatt et al. 2008b). The SMC is the only dwarf galaxy in the Local Group that has formed and preserved populous star clusters, without a significant age gap, across (most of) the age of the Universe, and the production has been prolific; Hodge (1986) estimates the SMC has some 2000 clusters.

Despite their utility and many clear advantages, SMC clusters have been surprisingly underexploited. The number of clusters with well-determined ages from deep main-sequence photometry is minimal. Only two clusters have had their detailed chemical abundances derived via high resolution spectroscopy (NGC 330 - Gonzalez & Wallerstein 1999, Hill 1999, NGC 121 - Johnson et al. 2004), and an additional six clusters have metallicities that were derived from Ca II triplet (CaT) spectroscopy of individual stars (Da Costa & Hatzidimitriou 1998, hereafter DH98). Aside from these eight clusters, all other existing abundance determinations are based only on photometry or integrated spectroscopy. Thus, the really detailed information, viz. accurate ages and abundances, necessary to fully utilize SMC clusters, both as tracers of the SMC's formation and chemical

evolution history, and as templates for studying stellar populations in more distant galaxies, is sorely lacking.

Our group has been working to ameliorate this situation over the past several years. Using Washington photometry, we have derived ages and metallicities for almost 50 previously unstudied or poorly studied clusters (Piatti et al. 2001, 2005a, 2007a,b,c). These results have greatly improved our understanding of the global properties of the SMC cluster system, provided constraints on the age-metallicity relation (AMR), explored possible gradients, cluster formation scenarios, etc. However, these photometric cluster ages and abundances suffer from two problems. First, our photometry comes from data obtained with a 1m class telescope, which is barely adequate to reach the main sequence turn off for clusters older than several Gyr at the distance of the SMC. Second, while the photometry for the red giant stars that are used to derive cluster abundances is generally good, the Washington technique is known to require a significant age correction to metallicities derived for intermediate-age ($\lesssim 5$ Gyr) objects (Geisler et al. 2003), an age range that includes the majority of the SMC clusters so far observed. This is of course illustrative of the infamous age-metallicity degeneracy and is not a problem restricted to the Washington system; while some age and metallicity estimates from isochrone fitting to CMDs constructed in other photometric systems exist, the degeneracy between age and metallicity also makes these estimates inherently uncertain in the absence of more solid metallicity measurements based on spectroscopic data.

As mentioned above, spectroscopic based abundances only exist for a handful of SMC clusters, with most of the sample coming from the work by DH98. They combined their CaT based metallicities with ages from the literature to create the first accurate AMR for the SMC, and found that it was consistent with a simple closed box model and did not require the significant gas infall or strong galactic winds that were needed to explain

previous SMC AMR’s (e.g., Dopita 1991). In addition, DH98 found that their cluster velocities, like other kinematic tracers in the SMC, show no evidence for any systematic rotation of the SMC. However, their small sample size and large age errors severely limit how well we can constrain the kinematics and chemical evolution of the SMC.

While the CaT method does not measure Fe abundances directly, previous authors have shown that the strength of the CaT lines are an excellent proxy for $[\text{Fe}/\text{H}]$, and can be used in stellar populations covering a wide range of ages and abundances (e.g., Cole et al. 2004; Carrera et al. 2007). An added benefit of using the CaT is that it is very efficient; not only are RGB stars near their brightest in the infrared, but the multiplexing capabilities of many moderate-resolution spectrographs allows the observation of dozens of stars simultaneously, greatly increasing the probability of identifying cluster members. In a previous paper (Grocholski et al. 2006, hereafter G06), we have applied this method to the LMC with excellent results, following up on the pioneering work by Olszewski et al. (1991). Using FORS2 on the VLT, we were able to identify more than 200 member stars in 28 populous LMC clusters and determine accurate mean cluster velocities ($\sigma = 1.6 \text{ km s}^{-1}$) and metallicities ($\sigma = 0.04 \text{ dex}$) and use these to explore the global cluster metallicity distribution, kinematics, etc.

To further refine our knowledge of the velocities and abundances of clusters in the SMC, we here apply this powerful technique to the SMC, again using FORS2 on the VLT to obtain medium-resolution near-infrared spectra of the CaT lines in 270 individual RGB stars in and around 16 SMC clusters. Herein we present our efforts to identify cluster members and derive mean abundances and velocities for these clusters. In a future paper we will analyze the several hundred field stars that were also observed as part of this project. This paper is organized as follows: In §2, we describe our target selection process, and our spectroscopic observations and reduction procedures are detailed in §3.

In §4 and §5, we present the radial velocities and equivalent width measurements and the metallicity derivation, respectively. The membership selection process is described in §6 and §7 compares our metallicity values with previous determinations. In §7 we also discuss our metallicity results and in §8 the kinematics. Finally, in §9 we summarize our results.

2. Target Selection

To significantly improve upon the work of DH98, we have observed 16 SMC clusters. Our cluster sample was chosen based on our Washington photometry, where we have targeted clusters that appear to be at least as old as 1 Gyr (this is approximately the minimum age for which CaT is well-calibrated), and cover as large a range in ages as possible so as to sample the AMR over a wide baseline. We note that our clusters were chosen to be complementary to those of DH98, as well as a similar study by Kayser et al. (2009, in preparation), whose targets we were aware of. The ages of all but one of our clusters have been derived from Washington photometry, using both the magnitude difference between the red clump (RC) and the main sequence turn off (Geisler et al. 1997) as well as fitting isochrones. For L 17, we only had preliminary Washington photometry and instead used the age derived by Rafelski & Zaritsky (2005), which is based on integrated UBVI photometry. We also attempted to select clusters that were in relatively uncrowded fields and that were spread around the galaxy so as to cover as wide an area and radial range as possible in order to search for any global effects such as gradients. Finally, we preferred clusters that were not too centrally condensed and with a reasonable number of giants in order to allow us to observe at least four definite cluster members from which to derive the cluster metallicity. In Table 1, we list our target clusters along with their various catalog designations, right ascension, and declination.

In Figure 1 we show the position of our cluster sample and the clusters observed by

DH98, in relation to the optical center and bar, as well as several ellipses aligned with the bar demonstrating our method for deriving the galactocentric distance of a cluster (see section 7.3). The sample covers a significant fraction of the galaxy.

DH98 studied 7 SMC clusters but they report the metallicity of only 6 of them, because NGC 361 did not have suitable photometry at the time their work of DH98 was published.

V- and *I*-band pre-images of our target fields were taken by ESO Paranal staff in 2005 August as part of Program 076.B-0533. In all cases except one, the cluster was centered on the upper (master) CCD, while the lower (secondary) CCD was used to observe only field stars. In the case of BS 121, the instrument was rotated in order to center BS 121 on the master CCD and include the nearby cluster L 72 on the secondary CCD. Unfortunately, L 72 turned out to be only a 25 Myr old cluster (Piatti et al. 2007a), therefore, all RGB stars observed around this cluster are actually SMC field stars. The pre-images were processed within IRAF ¹, and stars were identified and photometered using the aperture photometry routines in DAOPHOT (Stetson 1987). Stars were cataloged using the FIND routine in DAOPHOT and photometered with an aperture radius of 3 pixels. The *V* and *I* band data were matched to form colors. We note that these exposures were purposefully lengthened in order to go deep enough to reach below the main sequence turnoff for most of our clusters and in a future paper we will present the full point spread function fitting photometry and the resulting cluster ages, based on isochrone fitting to our data.

Spectroscopic targets were chosen based on the instrumental CMD, giving highest priority to stars lying along the apparent cluster giant branch. Each candidate was visually inspected to ensure location within the cluster radius (judged by eye) and freedom

¹Image Reduction and Analysis Facility, distributed by the National Optical Astronomy Observatories, which is operated by the Association of Universities for Research in Astronomy, Inc., under contract with the National Science Foundation.

from contamination by very nearby bright neighbors. In each cluster we then looked for maximum packing of the $\approx 8''$ -long slits into the cluster area and for the best possible coverage of the magnitude range from the horizontal branch/red clump ($V \approx 19.5$) to the tip of the RGB ($V \approx 17$) in order to select the best cluster targets. The positions of each target were defined on the astrometric system of the FORS2 pre-images so that the slits could be centered as accurately as possible, and the slit identifications were defined using the FORS Instrument Mask Simulator (FIMS) software provided by ESO; the slit masks were cut on Paranal by the FORS2 team. In general we were able to place slits on some 10 stars per cluster that we judged initially to be likely members based on their location and photometry. This left ample additional space for other targets, both on the master chip and especially on the secondary chip, and we selected as many field giants as possible in order to explore their metallicities and kinematics as well. Typically we observed about 25 probable field giants around each cluster.

3. Spectroscopic Observations and Reductions

The spectra of the program stars were obtained during 2005 November in service mode by the VLT staff, using the FORS2 spectrograph in mask exchange unit (MXU) mode. Our instrumental setup was identical to that discussed in G06, which can be consulted for a more detailed description. We used slits that were $1''$ wide and $8''$ long. In all fields, we obtained a single 900 s exposure with a typical seeing of less than $1''$. Pixels were binned 2×2 , yielding a plate scale of $0.25'' \text{ pixel}^{-1}$. The spectra have a dispersion of $\sim 0.85 \text{ \AA/pixel}$ (which corresponds to a resolution of 2-3 \AA) with a characteristic rms scatter of $\sim 0.06 \text{ \AA}$, and cover a range of $\sim 1600 \text{ \AA}$ in the region of the CaT (8498 \AA , 8542 \AA and 8662 \AA). S/N values ranged from ~ 10 to $\sim 70 \text{ pixel}^{-1}$. Calibration exposures, bias frames and flat-fields were also taken by the VLT staff.

We followed the image processing detailed in G06. In brief, we used the IRAF task *ccdproc* to fit and subtract the overscan region, trim the images, fix bad pixels, and flat-field each image. We then corrected the images for distortions, which rectifies the image of each slitlet to a constant range in the spatial direction and then traces the sky lines along each slitlet and puts them perpendicular to the dispersion direction. We used the task *apall* to define the sky background and extract the stellar spectra onto one dimension. The tasks *identify*, *refspectra* and *dispcor* were used to calculate and apply the dispersion solution for each spectrum. Finally, the spectra were continuum-normalized by fitting a polynomial to the stellar continuum. Two examples of the final spectra in the CaT region can be seen in Figure 2. Clearly, the three Ca II lines dominate the red giant’s spectra in this region. Also note the stronger Ca lines in the bottom spectrum, which, given the very similar T_{eff} and $\log g$ values (as indicated by their virtually identical $v - v_{HB}$ values), graphically illustrates the higher metallicity of the bottom spectrum and the power of the CaT technique.

4. Radial Velocity and Equivalent Width Measurements

Radial velocities (RVs) of our target stars are useful for evaluating cluster membership since it is expected that SMC stars have substantially higher RVs than foreground MW stars and that the cluster’s velocity dispersion should be small in comparison to that of the surrounding SMC field stars. In addition, the program used to measure the EWs of the CaT lines needs to know the RV in order to make the Doppler correction and to derive the CaT line centers.

To measure RVs of our program stars, we performed cross-correlations between their spectra and the spectra of 32 bright Milky Way open and globular cluster template

giants using the IRAF task *fxcor* (Tonry & Davis 1979). We used the template stars of Cole et al. (2004, hereafter C04) who observed these stars with a setup very similar to ours. The template spectra correspond to 2 stars each from Melotte66 and NGC 2298, 3 stars each from NGC 4590, Berkeley 20 and 47 Tuc, 6 stars each from NGC 1904 and Melotte 67 and 7 stars from Berkeley 39. In addition, *fxcor* makes the necessary correction to place the derived RV in the heliocentric reference frame. We adopted the average of each cross-correlation result as the heliocentric radial velocity of a star, finding a typical standard deviation of $\sim 6 \text{ km s}^{-1}$.

As shown in previous papers (e.g., Irwin & Tolstoy 2002), errors in centering the image in the spectrograph slit can result in inaccuracies in determining RVs. In order to correct for this, we measured the offset Δx between each star’s centroid and the corresponding slit center by inspecting the through-slit image taken immediately before the spectroscopic observation, according to the procedures described by C04 and G06. Then, the velocity correction Δv will be:

$$\Delta v = \Delta x \frac{dv}{dx}, \quad (1)$$

where $\Delta x = x_{cen}(slit) - x_{cen}(star)$ and dv/dx is our spectral resolution.

Typical centering errors are no larger than 0.90 pixels and our measurement precision is estimated to be 0.15 pixels. Given our spectral resolution of $\sim 30 \text{ km s}^{-1} \text{ px}^{-1}$, the velocity corrections we have applied range from $|\Delta v| = 0$ to 27 km s^{-1} and the typical error introduced in the RV turns out to be $\pm 4.5 \text{ km s}^{-1}$. This error, added in quadrature to the one resulting from the cross-correlation, yields a total error of 7.5 km s^{-1} . This value has been adopted as the typical RV error (random + systematic) of an individual star.

To measure EWs we have used a previously written FORTRAN program (see C04 for

details). The region around the CaT is highly contaminated by weak absorption lines, so we follow the procedure of Armandroff & Zinn (1988) and define continuum bandpasses on both sides of each CaT line. The rest wavelength of the CaT line centers, along with the continuum bandpasses that we have adopted from Armandroff & Zinn (1988), are listed in Table 2 of G06. For RGB stars, the flux in the wavelength range around the CaT is virtually flat, so the “pseudo-continuum” for each CaT line is then easily determined by a linear fit to the mean value in each pair of continuum windows. The “pseudo-equivalent width” is calculated by fitting a function to each CaT line with respect to the pseudo-continuum. Following C04 and G06, we define our metallicity index, ΣW , as the sum of the EWs of the three CaT lines. As discussed by Rutledge et al. (1997b) and C04, just fitting a Gaussian (G) function to the very strong CaT lines tends to underestimate the strength of the wings of the line profile, especially at high metallicity. C04 found that, by adding a Lorentzian profile to the Gaussian (GL), it is possible to maintain sensitivity over the full range of abundances. However, C04 also showed that, by adding artificial noise to one of their spectra, for stars with S/N less than ~ 15 -20, there is no significant difference in the EWs measured using the two profile shapes. In light of this, for spectra with S/N > 20 , we use the composite line fits (GL), but for spectra with S/N < 20 , we prefer a Gaussian-only fit, since it has fewer free parameters. We correct the Gaussian-only fit for the low S/N spectra as follows. We measured ΣW for the spectra with high S/N (> 20) using both a Gaussian (ΣW_G) and a Gaussian+Lorentzian (ΣW_{GL}) function. In Figure 3 we plot ΣW_G vs. ΣW_{GL} , and find a best-fit linear relation:

$$\Sigma W_{GL} = \frac{\Sigma W_G - 0.280}{0.848}, \quad (2)$$

with a scatter of 0.23 \AA . Then, for low S/N (< 20) spectra, we measured the EW using G-fits, calculated ΣW_G and then calculated via equation (2) the corresponding ΣW_{GL} .

Errors in the EW measurements were estimated by measuring the rms scatter of the data about the fits, and yielded typical errors of $\sim 0.1\text{-}0.5 \text{ \AA}$ depending on the line and the S/N of the spectra. To calculate the errors involved in the ΣW calculation, we added in quadrature the error of the EW of each of the three lines. In the case of those spectra with $S/N < 20$ this last error was added in quadrature with the scatter of equation (2). Note that C04 also derived a linear relation between ΣW_G and ΣW_{GL} using galactic open and globular cluster stars. They found a change in the slope at $\Sigma W_{GL} \approx 6.5 \text{ \AA}$. There is no strong evidence of this slope change in our data.

5. Metallicities

Several studies have calibrated the relationship between the strengths of the CaT lines and stellar abundance. In all cases, the selected CaT index uses a linear combination of the EW of two or three individual Ca II lines to form the line strength index ΣW . For example, Suntzeff et al. (1993) and Cole et al. (2000) used a linear combination of the two strongest lines (8542 \AA and 8662 \AA), while in other cases all three lines were used, but each line was assigned a different weight in deriving the sum (e.g., Rutledge et al. 1997a). Since our spectra are of high enough quality that all three CaT lines are well measured, we adopted for ΣW the same definition as C04, in which all three lines are used with equal weight, namely:

$$\Sigma W = EW_{8498} + EW_{8542} + EW_{8662}, \quad (3)$$

Although theoretical and empirical studies have shown that effective temperature, surface gravity, and $[\text{Fe}/\text{H}]$ all play a role in CaT line strengths (e.g., Jørgensen et al. 1992; Cenarro et al. 2002), Armandroff & Da Costa (1991) showed that there is a linear

relationship between a star’s absolute magnitude and ΣW for red giants of a given metallicity. Following previous authors, we then define a reduced equivalent width, W' , to remove the effects of surface gravity and temperature on ΣW via its luminosity dependence:

$$W' = \Sigma W + \beta(V - V_{HB}), \quad (4)$$

in which the introduction of the difference between the visual magnitude of the star (V) and the cluster’s horizontal branch/red clump (V_{HB}) also removes any dependence on cluster distance and interstellar reddening. The value of β has been investigated by previous authors and we have adopted the value obtained by C04: $\beta = 0.73 \pm 0.04$. We chose C04’s value of β because they used both globular and open clusters, covering a range of ages similar to the clusters in our sample, to derive it and their instrumental setup is very similar to ours. We note that, as discussed in detail in G06, the use of C04’s value for β , combined with defining the brightness of our target RGB stars relative to the HB of their parent cluster, incorporate any age effects into the CaT calibration, thus it is not necessary to make any corrections for the ages of our clusters. As shown by Rutledge et al. (1997a), there is a linear relationship between a cluster’s reduced EW and its metallicity on the Carretta & Gratton (1997) abundance scale for globular clusters of the Milky Way. C04 extended this calibration to a wider range of ages ($2.5 \text{ Gyr} \leq \text{age} \leq 13 \text{ Gyr}$) and metallicities ($-2.0 \leq [\text{Fe}/\text{H}] \leq -0.2$) by combining the metallicity scales of Carretta & Gratton (1997) and Friel et al. (2002) for globular and open clusters, respectively. Although some of our clusters are younger than 2.5 Gyr, we adopted the C04 relationship,

$$[\text{Fe}/\text{H}] = (-2.966 \pm 0.032) + (0.362 \pm 0.014)W', \quad (5)$$

to derive the metallicities of our entire cluster sample. Carrera et al. (2007) investigated the behaviour of CaT in the age range of $0.25 \text{ Gyr} \leq \text{age} \leq 13 \text{ Gyr}$ and the metallicity range

$-2.2 \leq [\text{Fe}/\text{H}] \leq +0.47$. In spite of the extended age range of their calibration, we decided to use C04’s calibration for three reasons. First, the calibration of Carrera et al. (2007) uses the absolute magnitude of a target star (rather than the brightness relative to the HB, as we have adopted), thus requiring accurate photometric calibration and distance to the star. Unlike the LMC, the SMC and its cluster system is substantially extended along the line of sight (e.g., Crowl et al. 2001; Glatt et al. 2008b), making it difficult to determine the distance to an individual cluster, thereby introducing an additional source of error in our calculation. Second, using $(V - V_{HB})$ instead of absolute magnitude removes the need to make any assumptions about the foreground reddening toward a cluster. Finally, Carrera et al. (2007) performed estimates of the differences in W' as a function of age using the Jørgensen et al. (1992) models and *BaSTI* stellar evolution models (Pietrinferni et al. 2004). From their data, they confirmed that the influence of age is small, even for ages < 1 Gyr. Based on this result, we are confident that the C04 calibration can be accurately extended to younger ages. Note that our youngest clusters are estimated to be ~ 0.9 Gyr (Lindsay 106 and 108), but the rest are $\gtrsim 1$ Gyr.

In addition, Battaglia et al. (2007) have shown that $[\text{Fe}/\text{H}]$ values derived from CaT agree with those from high resolution spectroscopy and detailed model atmosphere analyses to within 0.1 - 0.2 dex over the range $-2.5 \leq [\text{Fe}/\text{H}] \leq -0.5$, based on FLAMES data for a large sample of stars in the Sculptor and Fornax dwarf spheroidal galaxies. It is well known that such stars have distinct $[\text{Ca}/\text{Fe}]$ ratios from those in the Galactic globular cluster calibrators (e.g., Shetrone et al. 2001; Geisler et al. 2007) and also possess a larger range of stellar ages, extending to much smaller values. Nevertheless, CaT yields metallicities that are very close to real Fe abundances, reinforcing our confidence in the technique. Our estimate of the total metallicity error (random + systematic) per star ranges from 0.09 to 0.35 dex, with a mean of 0.17 dex.

6. Membership Selection

We generally follow the procedure described in detail by G06 to determine cluster membership, and give a brief description herein. As it is necessary to measure the HB/RC in each cluster, we begin by determining each cluster’s radius which will allow us to separate the cluster stars from the field to first order. One of the most robust ways to evaluate the cluster radius is using the stellar density radial profile, which we constructed following the method described by Piatti et al. (2007c). We start by determining the center of the cluster by building projected histograms in the x and y directions using the coordinates from the aperture photometry. Once this is performed, we fit Gaussian functions to the distributions using the task *NGAUSSFIT* of *IRAF*, adopting the derived values as the coordinates of the cluster’s center. Finally we constructed the cluster radial profile based on star counts within boxes of 50 pixels on a side distributed throughout the whole field of each cluster. The number of stars per unit area at a given radius can be calculated through the expression given by Piatti et al. (2007c):

$$\frac{n_{r+25} - n_{r-25}}{(m_{r+25} - m_{r-25})50^2}, \quad (6)$$

where n_r and m_r are the number of stars and boxes in a circle of radius r , respectively. We adopted as the cluster radius the value where the gradient in the density profile significantly flattened. In Figure 4, we use L 19 to illustrate the process employed for all clusters. The x-axis represents the radial distance and the y-axis the number of stars (N) per unit area. The vertical line on the profile represents the adopted cluster radius, which is used in the subsequent analysis. Note that the adopted cluster radius can differ from the more typical definition, in which the radius is the distance from the center to the point where the stellar density profile intersects the background (Piatti et al. 2007c). As is seen in Figure 4, the background level is ~ 0.025 stars/arcsec². Thus, the real cluster radius probably extends

farther than the adopted one. We decided to use for our analysis a conservative radius in order to maximize the probability of cluster membership.

After defining the cluster radii, we build CMDs for each cluster using aperture photometry that is derived from our v - and i -band preimages. From here on, we denote our photometry with lower case letters to emphasize that these are presently uncalibrated instrumental values. We are able to make use of the instrumental photometry due to the fact that the $V - I$ color term is expected to be small in the FORS2 filter system (< 0.02 mag), and should therefore have little effect over the small range in colors covered by the RGB stars. Due to the fact that all of our clusters are too young and metal rich to have a fully formed HB, we instead adopt the median value of the core helium-burning red clump stars. The estimated change in v_{HB} from the old to the young populations is on the order of 0.05 dex (Grocholski et al. 2006) which is smaller than our measurement errors. All of the clusters in our sample show RC features that are well populated. We measure v_{HB} as the median value of all stars inside of a box that is 0.7 mag in v and 0.3 mag in $v - i$ and centered on the RC by eye. We use the median value instead of the mean since it reduces the effect of outliers on our calculations. Errors in v_{HB} are taken as the standard error of the median.

In Figure 5 we plot the xy positions of all stars photometered in and around L 19, and the corresponding CMD is plotted in Figure 6. Our spectroscopic targets are represented by the large filled symbols, and the adopted cluster radius is marked by the large circle in Figure 5. Target stars marked in blue are considered non-members due to their location outside of the adopted cluster radius but were still observed in order to study the SMC field population.

To further discriminate member from non-member stars, we can take advantage of the behavior of the radial velocities and metallicities as functions of clustercentric distance.

Cluster members should have a smaller velocity dispersion than field stars and may also have a mean velocity different from the field. Figure 7 shows how RV varies as a function of distance for L 19. We have adopted an intrinsic cluster velocity dispersion of 5 km s^{-1} , appropriate for typical Magellanic Cloud clusters (Pryor & Meylan 1993), which added in quadrature with our adopted radial velocity error of 7.5 km s^{-1} , yields an expected dispersion of $\sim 9 \text{ km s}^{-1}$. We have rounded this up and adopted $\pm 10 \text{ km s}^{-1}$ for our RV error cut, represented by horizontal lines in Figure 7. The vertical line represents the adopted cluster radius. Figure 8 plots metallicity versus distance from the cluster center for L 19. We have adopted an $[\text{Fe}/\text{H}]$ error cut of $\pm 0.20 \text{ dex}$ (horizontal lines) given our estimate of a typical metallicity error of 0.17 dex for an individual star. Again, the vertical line in Figure 8 marks the cluster radius. In both plots blue symbols represent non-members that are outside the cluster radius, teal and green symbols represent non-members that we eliminated because of discrepant radial velocity and metallicity, respectively, and red symbols are targets that have passed all three cuts and are therefore considered cluster members. This procedure is followed for each cluster in our sample.

In Table 2 we list the information for the member stars. Columns (1), (2) and (3) show the identification of the star, right ascension and declination respectively. Table 2 also lists heliocentric radial velocity and its error in columns (4) and (5), $v - v_{HB}$ in column (6), ΣW and its error in columns (7) and (8) and metallicity and its error in column (9) and (10). In Figure 9 we give the ΣW vs. $v - v_{HB}$ plot for all cluster’s members. Dashed lines represent isometallicity lines of $[\text{Fe}/\text{H}] = 0, -0.5, -1, -1.5$ and -2 (from top to bottom).

Finally, using these member stars, we calculated the mean cluster metallicity and its standard error of the mean. The final results are given in Table 3 where we list successively: cluster name, the number of stars, n , established as members, mean heliocentric radial velocity with its error, the mean metallicity followed by its error, position angle and the

semi-major axis a (see section 7.3 for details about the calculation of a). Both radial velocity and metallicity errors correspond to the standard error of the mean (s.e.m.). We derive the mean cluster metallicity (mean s.e.m., random error) to 0.05 dex and the mean radial velocities to 2.7 km s^{-1} for an average of 6.4 members per cluster. This compares well to the mean values we derived for our LMC cluster sample: 0.04 dex and 1.6 km s^{-1} for 8 stars, and is significantly better than the mean values obtained by DH98: 0.12 dex and 4.7 km s^{-1} for 4 stars per cluster (in a total of 6 clusters).

It is important to emphasize that the metallicity determination of BS 121 is more uncertain than for the other clusters due to the fact that it was difficult to select convincing metallicity cuts. The stars selected via radial velocity appeared to belong to two groups. The stars of the first group have metallicities similar to the field metallicity in that region (~ -0.95 dex) and are probably field stars. We therefore assumed that the lower metallicity group are the actual cluster members and used them to calculate the metallicity of BS 121. It is necessary to observe more stars in order to improve our metallicity uncertainty.

7. Metallicity Results

7.1. Comparison to Previous Metallicity Determinations and Sample Enlargement

Before investigating the implications of our metallicity results, it is first important to see how they compare with any previous determinations. Since our cluster sample is limited to only 15 clusters, in order to study global effects, obtain better statistical errors, etc., it would also be beneficial to enlarge the sample size as much as possible by including other studies whose metallicities we find to be on a similar scale to ours and also have relatively

small errors.

No previous CaT or high resolution spectra have been obtained for any of our clusters. The DH98 study, of course, includes several other clusters studied via CaT so we will add their sample to ours. Piatti et al. (2005b) did derive reddening and ages of L 5 and L 7 using low-resolution integrated spectra. However, the metallicities they report are not derived directly from their spectra.

Metallicities for a number of our clusters have been determined photometrically. Piatti et al. (2005a) presented results on the age and metallicity estimates of most clusters of our sample (BS 121, HW 47, HW 84, HW 86, L 4, L 5, L 6, L 7, L 19 and L 27) calculated from CMDs in the C and T_1 bands of the Washington system. The same technique was used by Piatti et al. (2007b) to derive the corresponding parameters for L 110.

Table 4 summarizes the previous photometric metallicity and age determinations for our clusters. Column (1) shows the cluster name, the metallicity and its respective error are found in column (2) and the age in column (3). Column (4) lists the reference from where the metallicities and ages were taken. There is no previous metallicity determination for the clusters L 17, L 72, L 106 and L 108. Note that we have used the ages derived from Washington photometry in all cases except L 17. These ages are based on main sequence photometry and have been determined using the same technique, thus assuring that they are on a homogeneous scale.

In Figure 10 we have plotted the metallicities derived by Piatti et al. (2005a, 2007b) as a function of the metallicities from the present work for the 11 clusters in common. We note that their metallicities for these clusters were derived by comparing the cluster red giant branches with those of fiducial globular clusters from Geisler & Sarajedini (1999) and then correcting the photometric metallicities for their age dependence via the prescription given in Geisler et al. (2003). The mean difference between our metallicities and those

derived by Piatti et al. (2005a, 2007b) is -0.04 ± 0.25 dex, with our values being more metal-rich, while a mean absolute difference of 0.20 ± 0.14 dex, for the 11 clusters in common, is found. The mean errors of the spectroscopic and photometric metallicities are 0.05 and 0.26 dex, respectively. Then the mean expected error (sum in quadrature of these two errors) is 0.27 dex, which is larger than the observed difference. Thus, our results are in good agreement with those derived from the Washington system. This indicates that the Washington photometric technique employed by Piatti et al. (2005a, 2007b) is well calibrated and especially that their correction for age effects is also appropriate. We further tested this latter point by plotting the difference in metallicity between the two studies vs. age (Figure 11). There is no systematic trend evident and the differences are within the range expected from the given errors except for BS 121, whose CaT metallicity is problematic. We conclude that the age correction procedure used in the Washington technique, outlined in Geisler et al. (2003), is indeed appropriate.

Although our spectroscopic metallicities and the photometric metallicities of Piatti et al. (2005a, 2007b) are consistent with each other, it is important to note that our CaT-based abundances are much more precise. As shown by the error bars in Fig. 10, our errors are < 0.07 dex while the photometric errors range from 0.2 to 0.4 dex. While this comparison gives us confidence that the photometric abundances from the Washington technique are on a similar scale to ours, the associated errors mean that their data are not precise enough to serve our purposes.

However, we can enlarge our sample size by including metallicities derived in several other studies which we deem to be essentially on the same scale as ours, although we have essentially no clusters in common. These studies include DH98 and any other clusters studied with the CaT technique, as well as any clusters studied with high resolution spectroscopy. For the DH98 clusters, we use the values they give in their Table 3 on the

Caretta & Gratton metallicity scale and uncorrected for age effects, as these are the closest to our scale. Note that their technique is not identical to ours as they used the sum of only the 2 strongest Ca lines, but the metallicities derived should be very similar. Glatt et al. (2008b) also give CaT metallicities for 3 additional clusters. We use their values on the Carretta & Gratton (1997) scale to match ours. Note that the errors associated with the mean cluster metallicities derived by both DH98 and Glatt et al. range from 0.06 – 0.13 dex, with a mean of 0.10 dex, twice as large as our mean error. However, we feel that these are good enough for our purposes. Finally, the only cluster with a metallicity based on high resolution spectroscopy published in a refereed journal to date is NGC 330 (Gonzalez & Wallerstein 1999), who derive -0.94 ± 0.02 for this very young cluster. We also add this derivation to our sample. This gives a total sample of 25 clusters with metallicities on a reasonably homogeneous scale and with relatively small errors.

7.2. Metallicity Distribution

The cluster metallicity distribution (hereafter MD) is an important diagnostic of the global chemical evolution of a galaxy and is useful for an overall comparison of the cluster systems of different galaxies. First, we derive a mean metallicity for our CaT sample of -0.94 , with σ (standard deviation) = 0.19, while for the full sample these values become -0.96 and 0.19. The mean values are in very good agreement with each other and the global mean value of -1 found by Carrera et al. (2008) from CaT spectra of a large number of field giants.

However, we note here that the ages for these clusters are not all on the same scale. Those for our sample are derived from Washington main sequence photometry but in some cases are based on isochrones and others based on the magnitude difference between the RC and turnoff, although these have been shown to give similar ages for clusters in common

(Geisler et al. 2003). DH98 adopted the ages given in the original CMD references for their cluster sample, which are based on MS photometry but vary in the details such as photometric system, age calibration, etc. Glatt et al. (2008b) use deep HST ACS photometry. Thus, the ages of our full sample are on a more heterogeneous scale than the metallicities. We are in the process of obtaining better ages for our own clusters based on a more sophisticated data reduction and analysis, i.e. psf-photometry of the (long exposure) preimages, but this is beyond the scope of the present paper. For this reason, we restrict our investigation utilizing the ages of our clusters to only the AMR. We feel it is premature to use the current age estimates to investigate properties that demand more homogeneous data, e.g., the fascinating question of whether or not there have been bursts of cluster formation, as first suggested by Rich et al. (2000) and more recently by Piatti et al. (2005a). Such analysis requires a larger and more homogeneous sample than currently available.

We can divide our sample into two age bins: younger and older than 3 Gyr. The 12 older clusters have a mean age of 5.8 Gyr and a mean metallicity of $-1.08, \sigma = 0.17$ (0.049 s.e.m.), while the 13 younger clusters have values of 1.6 Gyr, $-0.85, 0.15$ (0.041 s.e.m.). The two mean metallicities differ by 0.23 ± 0.06 dex (3.6 sigma). We feel, despite the caveats given above, that this difference is probably real and simply reflects the AMR discussed in detail below, in which we find that younger clusters are generally slightly more enriched. Note that the mean metallicity of even the younger division is still somewhat lower than that generally attributed to the present-day galaxy of ~ -0.65 (e.g., Russell & Bessell 1989; Hill 1997) as it includes objects of a few Gyr in age and there does appear to have been significant enrichment after this time (e.g., Harris & Zaritsky 2004; Carrera et al. 2008, and below). Particularly interesting in this regard is the youngest cluster in our combined sample, NGC 330, which at an age of $30 Myr$ has a metallicity of -0.94 .

The MD is shown in Figure 12 (top panel), in which we also show the MD for LMC clusters derived by G06 in our CaT study (bottom panel). The SMC clusters fall in a rather small metallicity range of < 0.8 dex, from -0.6 to -1.4 , and are concentrated in the 0.5 dex range from -0.75 to -1.25 . This is unlike the case of LMC clusters, which cover ~ 2 dex in metallicity (G06), with higher and lower metallicities than found in their SMC counterparts. G06 found that the older LMC clusters in their sample of 28 (very comparable to the present sample size) had metallicities (also based on CaT) from ~ -1.3 to -2.1 but that the younger clusters, which formed after the age gap ended some 3 Gyr ago, have a very tight MD, with a mean $[\text{Fe}/\text{H}] = -0.48$, $\sigma = 0.09$. The broad characteristics of the MD of the cluster systems of the Magellanic Clouds have been known for some time. Da Costa (1991) noted that (sic) “The LMC managed to make metals but no clusters during the age gap while the SMC managed to make clusters but no metals”. These curious facts are now even more evident and corroborated in much greater detail than known at that time, but their explanation remains as mysterious.

Piatti et al. (2005a) mention that their MD based on Washington photometry is suggestive of a bimodal distribution, with possible peaks around -0.8 and -1.25 . Our MD also hints at bimodality, with possible peaks around -0.9 and -1.15 , reasonably close to the values suggested by Piatti et al. The sample size is near the limit of drawing statistically significant results of this kind. Indeed, a KMM analysis (Ashman et al. 1994) indicates bimodality cannot be favored over unimodality with any statistical significance. Clearly, it is of great interest to enlarge the present sample in order to ascertain whether or not the SMC cluster MD is indeed bimodal.

7.3. Metallicity Gradient

Until recently, essentially nothing was known about the existence or not of any variation of metallicity with distance from the center of the SMC. Such metallicity gradients of course exist in many galaxy disks, including our own, and are well-traced by the cluster system (e.g., Janes 1979). However, Olszewski et al. (1991), Geisler et al. (2003) and G06 did not find any radial metallicity gradient in the LMC cluster system. Zaritsky et al. (1994) suggested that disk abundance gradients are ubiquitous in spiral galaxies, but that the presence of a classical bar tends to weaken the gradient. The LMC has such a bar, as does the SMC. Therefore, one might suspect that any metallicity gradient in the SMC may be weak if Zaritsky et al.’s idea is correct.

Previous searches for any gradient in the SMC have indicated the possible presence of a weak gradient. Piatti et al. (2007a) found a tendency for the mean cluster metallicity and its dispersion to be greater inside 4° than outside, and Piatti et al. (2007b) reinforced this finding. Carrera et al. (2008) studied CaT metallicities of a large number of field giants in each of 13 areas ranging from $1.1 - 3.9^\circ$ and found evidence for a significant metallicity gradient. More specifically, they found that the areas within $\sim 2.5^\circ$ have a relatively constant mean metallicity of ~ -1 but that this value decreases in their outermost fields, down to ~ -1.6 near 4° . They noted that this gradient could be due to either a chemically less-evolved outer region or a similar chemical evolution (essentially AMR) throughout the galaxy but with a varying mix of ages, with a larger fraction of younger, more metal-rich stars closer to the center, or both, and suggested the second scenario is most likely.

In order to investigate any gradient, one must first address the orientation of the galaxy and projection effects. In the LMC, the orientation of the galaxy is well-determined and distances can be deprojected to derive true galactocentric distances. However, the orientation of the SMC is much more poorly determined and it is also significantly elongated

along the line of sight, making determination of true galactocentric distances much more problematic. Following Piatti et al. (2007a), in an effort to derive galactocentric distances more accurately than simply ignoring projection effects, we adopted an elliptical coordinate system with $b/a = 1/2$ and aligned along the Bar, as shown in Figure 1. This reference system appears more appropriate for deriving galactocentric distances than a system simply aligned along the cardinal directions. We computed for each cluster the value of the semimajor axis, a , that an ellipse would have if it were centered on the SMC center, aligned with the Bar, had a b/a ratio of $1/2$ and one point of its trajectory coincided with the cluster position, and use this as a surrogate for the true galactocentric distance. We give the a value so derived for each cluster in Table 3.

In Figure 13 we plot metallicity vs. the semi-major axis a value for our cluster sample and for the full sample. No clear trend is evident. Dividing our sample at 4° , as did Piatti et al. (2007a,b), we find for the 15 inner clusters a mean metallicity and standard deviation of -0.94 , 0.19 , while the 10 outer clusters have -1.00 , 0.21 . The difference is not significant. To check to see if this could possibly be due to an inverse age gradient effect, we also checked the mean ages of the two divisions. The inner clusters are 3.1 (1.9) Gyr and the outer clusters 4.4 (3.4) Gyr. Thus, this can not be the cause of a lack of an observed metallicity gradient. We conclude that any true metallicity gradient in the SMC cluster system must be relatively weak. Note that our clusters extend to distances twice as far from the center as Carrera et al’s field star sample. It is unclear why they found a gradient and we do not. Obviously, these intermediate-age clusters and field stars may now occupy a position in the SMC quite distinct from that where they were born. Additional data are required to ascertain the existence and strength of any gradient. If the gradient is indeed minimal, Zaritsky et al. (1994)’s suggestion that a strong bar weakens any disk gradient is a viable explanation.

7.4. Age-Metallicity Relation

One of our best clues into the detailed chemical evolutionary history of a galaxy is provided by the relationship between the age of a population and its overall metallicity and how it varies with time. This AMR can be compared to models incorporating a variety of variable parameters concerning the chemical evolution to test their importance. Clearly, both the ages and metallicities of the tracer population need to be as accurately determined and on as homogeneous a scale as possible.

There have been a number of investigations aimed at deriving the SMC AMR using various stellar populations, including star clusters, field giants and planetary nebulae. The earliest studies by Stryker et al. (1985), Da Costa (1991) and Olszewski et al. (1996) generally agreed on several salient points: 1). There was an initial period of quite rapid enrichment which brought the metallicity up to ~ -1.2 , the metallicity (DH98) of the only old “globular cluster” in the SMC, NGC 121, by the time of its formation some 11 Gyr ago (Glatt et al. 2008a). Note that this phase is not well traced - it is simply based on the fact that the oldest cluster was formed from material that had already achieved this level of enrichment. Indeed, in the latest work with PNe (Idiart et al. 2007), they find metallicities ~ -1 for the oldest planetaries in their sample, with ages approaching the age of the universe, again demonstrative of the rapidity of this earliest enrichment phase. 2). For the next ~ 8 Gyr, the enrichment was quite slow, although both clusters (Da Costa 1991) and field stars (Harris & Zaritsky 2004) were formed in significant numbers. 3). Finally, during the past several Gyr, the enrichment has proceeded at a substantially quicker pace, bringing the global metallicity up to its current value of ~ -0.65 (Russell & Bessell 1989).

Thus, prior to the work of DH98, it appeared that the enrichment during the intermediate age period was very small and that the enrichment in the last few Gyr was especially dramatic. This sort of AMR is very different from that in the solar neighborhood

as well as that expected from the simple “closed box” model of chemical evolution, in which star formation proceeds gradually and hence abundances change slowly. In order to account for such effects, one needs to invoke infall of unenriched gas or outflow of processed gas in a galactic wind, or possibly a burst of star and cluster formation, which complicate the chemical evolution.

DH98 obtained the first well constrained AMR of SMC clusters, based on CaT spectra and deep CMD ages. However, their sample size was small – only 6 clusters – so they augmented it with data from other sources (as we do). They observed four intermediate-age clusters and found that the two oldest, L1 and K3, are slightly more metal rich than the two youngest, L113 and NGC 339. They argued that the AMR derived from L1 and K3 plus their other clusters was the true global AMR and that L113 and NGC339 were “anomalous” and required an additional explanation, such as infall of metal-poor gas. The AMR derived from the other objects yielded a smooth, continuous enrichment throughout the history of the galaxy, with no change in the rate of increase in the last few Gyr. According to them, the metallicity increased from ~ -1.2 to ~ -0.75 between $\sim 10 - 3$ Gyr, and continued to increase at a slightly smaller rate in the last 3 Gyr. They found that a simple closed box model (shown in Figure 14 as the short dashed curve) fit their data well (with the exception of the 2 problematic clusters) and that neither infall nor outflow of gas nor any discontinuous process was required for the global trend. However, note that their conclusions would change substantially if they instead considered L1 and K3 as anomalous, in which case their AMR would resemble much more those of previous studies, with a much slower enrichment during the intermediate period.

Subsequent AMR investigations have tended to corroborate the original studies and reinforce the need for something more complicated than the simple model proposed by DH98. In a series of papers investigating cluster ages and abundances from Washington

photometry, currently culminating in Piatti et al. (2007c), Piatti and collaborators compiled this information for a total of almost 50 clusters. Their AMR clearly shows very little enrichment in the intermediate period and substantial enrichment beginning about 3 Gyr ago. This result is in excellent agreement with the model of Pagel & Tautvaišienė (1998, hereafter PT98) which assumes an early burst, followed by no star formation from $\sim 12 - 4$ Gyr ago, and then an ensuing burst of recent star formation, leading to a significantly enhanced subsequent enrichment. The PT98 AMR is shown in Figure 14 as the solid curve. Using the *UBVI* photometry from their Magellanic Clouds Photometric Survey, Harris & Zaritsky (2004) derived the AMR for both field stars and clusters in the SMC and found the two AMRs to be consistent with each other. Their final relation, shown in Fig. 14 as a dotted line, is similar to the PT98 AMR for younger ages but has substantially enhanced metallicities for ages > 2 Gyr. Note that the Harris & Zaritsky (2004) study was not sensitive to objects older than 10 Gyr. Based on 29 PNe, Idiart et al. (2007) built an AMR that is similar to that of Harris & Zaritsky but offset to even higher metallicities in the intermediate age range by ~ 0.2 dex and shows virtually no change in metallicity during this period. Noël et al. (2007) determined the AMR for a field 1.1° to the southeast of the SMC center using *B*- and *R*- band photometry and a detailed analysis including isochrones and the star formation history. Their AMR is corroborated in an independent study by Carrera et al. (2008), which includes some fields in common with Noël et al. (2007). Carrera et al. (2008) used the CaT to derive metallicities on the CG97 scale for a large number of field giants in regions spread across the SMC. They find the AMRs for each region are indistinguishable and that there is thus a global AMR. We plot the mean age and metallicity points from Carrera et al. (2008) in Fig. 14 (open squares) along with the derived best-fit model (long dashed curve). The model, which comes from Carrera (2005), did not assume any bursts but instead used both infall and outflow.

Our clusters are presented in Figure 14, along with the additional samples described

above. A summary of the ages and metallicities that we are considering for these samples, as well the corresponding references, is given in Table 5. The overall agreement with the PT98 model is good, albeit there are two regions of disagreement. The predicted metallicity is generally lower than observed from 5 – 10Gyr, and our 4 youngest clusters as well as NGC 330 are significantly more metal-poor than the PT98 prediction. DH98’s 2 “anomalous” clusters (which have exactly the same assigned age and metallicity) are now very well behaved with respect to the PT98 model and in fact it is L 1 and K 3 which appear anomalous (too metal-rich)! Note that the ages of all of the DH98 clusters have changed in Glatt et al. (2008b)’s derivation and should be much better determined now. We therefore adopt the ages of Glatt et al., which are derived via main sequence fitting with the Dartmouth isochrones. As pointed out by Glatt et al. (2008b), a small age gap in the cluster distribution now appears between the oldest SMC cluster (NGC 121 =10.5 Gyr) and the second oldest cluster (L1 at 7.5 Gyr). This is much briefer than the infamous LMC cluster age gap, where only 1 cluster is found to have an age between 12 – 3Gyr. Curiously, this lone LMC age-gap cluster was formed in the middle of the SMC “age gap”. In any case, the SMC gap appears real and is interesting, and no subsequent gaps of more than a Gyr appear. The very minimal chemical enrichment predicted by PT98 in the intermediate period and the fast and continuing rise starting about 3 Gyr ago are particularly well reproduced by the data (with the exception of the youngest clusters). Note that L 11, the DH98 point at (3.5 Gyr, -0.75), has a CaT value estimated by Kayser et al. (2006) to be ~ -0.9 , which would bring it more in line with the PT98 prediction. The Carrera model gives a similarly good overall fit, especially in the two regimes where the PT98 model is poorest.

Thus, our data are in good overall agreement with the PT98 burst model, as well as with the hybrid infall + outflow model of Carrera (2005). The ideal model would predict metallicities between these 2 models. It is clear that something more complex

than the simple closed box model of DH98 is required to explain the observations: the rate of enrichment during the intermediate period was certainly much less than over the last few Gyr. In fact, the metallicity appears to have stayed almost constant at ~ -1.1 from 10 – 3Gyr and then had a later increase. Our data are also in very good agreement with Carrera et al.’s field star data, indicating, as they first discovered, that the AMR was universal. We will focus our discussion on the burst model.

The possibility of a burst of star formation to explain the AMR in the SMC was first suggested by Tsujimoto et al. (1995) and developed by PT98. They assumed a burst at 4 Gyr, partly based on the AMR’s available to them. Note that their model includes infall of unprocessed material as well. A problem with their burst model is that they predict no star formation from 12 – 4 Gyr, although it is clear this was NOT the case and that an important fraction of both the stellar and cluster populations were formed during this period (e.g., McCumber et al. 2005; Da Costa 1991). Rich et al. (2000) argued from HST imaging for 7 clusters that there were 2 main epochs of cluster formation: one at 8 ± 2 Gyr and another at 2 ± 0.5 Gyr, and that the metallicities of the clusters in each group are also very similar. Piatti et al. (2005a, 2007b), from a much larger sample of clusters but with less precise age determinations, suggested possible bursts at about these same times. Note that such bursts could possibly explain the metallicity bimodality if it is real. Harris & Zaritsky (2004) found peaks in the age distribution at 0.4 and 2.5 Gyr in the global field star formation history but no significant peaks in the cluster age distribution. Idiart et al. (2007) also claimed their AMR supported a burst that occurred in the last 2 – 3 Gyr and that there was very little chemical evolution before this time going back to > 10 Gyr ago.

The case for reduced star formation and chemical enrichment during the intermediate period from $\sim 10 - 3$ Gyr and a recent period of enhanced star formation and enrichment

over the last few Gyr is well supported by a preponderance of the data currently available, including our own. The question obviously arises as to what caused the recent burst? Bekki et al. (2004) analyzed the orbits of the Magellanic Clouds and concluded that the first close encounter between them occurred about 4 Gyr ago and this could have led to strong triggering of star and cluster formation. Unfortunately, our current knowledge of the Clouds' proper motions prohibits us from making definitive statements or prediction, and indeed the most recent values all suggest the Magellanic Clouds may be unbound to each other and only beginning their first close encounter to the MW (Kallivayalil et al. 2006; Piatek et al. 2008). Note that the LMC also experienced a recent burst at approximately the same time but clusters born over the last few Gyr show a very uniform metallicity, with no signs of the metallicity increase that most of their SMC cousins underwent. G06 find that their sample of 23 LMC intermediate-age clusters (1 – 3 Gyr old) have a very tight metallicity distribution, with a mean of -0.48 and a standard deviation of only 0.09 dex. In our SMC sample, the 10 clusters in the same age range have a mean of -0.82 and $\sigma = 0.15$, and thus are both significantly more metal-poor and with a wider metallicity spread than their LMC counterparts. Clearly, more high quality ages and metallicities, as well as detailed elemental abundances, for SMC clusters are required to help constrain its chemical evolution.

8. Kinematics

The structure of the SMC is known to be extremely complex, with a large line-of-sight depth that may vary across the face of the SMC (e.g., Crowl et al. 2001), possibly a result of interactions with the LMC and Galaxy. Some studies of the SMC's kinematics suggest that they may be equally complex. For example, Stanimirović et al. (2004) used H I observations to examine the kinematics of the SMC and found what appears to be

differential rotation, with a turnover radius of ~ 3 kpc. The authors suggest that the central region of the SMC may correspond to a disk-like structure left over from when the SMC was rotationally supported, a time prior to any interactions with the LMC and MW.

Other authors, however, did not find evidence of rotation. Harris & Zaritsky (2006) summarized previous radial velocity studies of the SMC. As seen in their Table 3, these are based on the study of a variety of different objects, including planetary nebulae (Dopita et al. 1985), red giant stars (Suntzeff et al. 1986; Harris & Zaritsky 2006), supergiants and main sequence stars (Maurice et al. 1987), cepheids (Mathewson et al. 1988), carbon stars (Hardy et al. 1989; Hatzidimitriou et al. 1997), red clump stars (Hatzidimitriou et al. 1993) and expanding H I shells (Staveley-Smith et al. 1997). The mean heliocentric radial velocities (ranging from 123 to 162 km s⁻¹) and velocity dispersions (ranging from 18 to 33 km s⁻¹) are in good agreement, regardless of the type of tracer used in the analysis. From analysis of their own data (2046 SMC stars in 16 fields), Harris & Zaritsky (2006) found a velocity gradient that may include a signature of rotation in the SMC. They found an apparent rotation amplitude of 8.3 km s⁻¹ deg⁻¹ and a rms scatter of 27.5 ± 0.5 km s⁻¹.

More recently, Carrera (2005), obtained similar results with stars in 13 fields of the SMC. He observed that the velocities are compatible with the presence of a small rotation, with an amplitude of 30 ± 4 km s⁻¹ and maximum radial velocity at PA $\sim 150^\circ$. However, both Carrera and Harris & Zaritsky, noted that part or all of this “rotation” could in fact be due to the projected tangential motion of the galaxy. Given that the possible rotation velocity is much smaller than the velocity dispersion, both concluded that the SMC is primarily supported by its velocity dispersion.

Regarding star clusters, the only previously published work is that of DH98, who used their CaT spectra to obtain radial velocities of seven SMC clusters. They found a mean

radial velocity of $138 \pm 6 \text{ km s}^{-1}$ and a velocity dispersion of $16 \pm 4 \text{ km s}^{-1}$, values in reasonable accord with those summarized above. From their analysis, they support the conclusion of the lack of evidence for any systematic rotation of the SMC.

To test for global rotation, we have analyzed the behaviour of the cluster radial velocities derived by us as a function of position angle. The velocity data of our sample are plotted in Figure 15 (solid circles). To calculate the position angle we have used the equations of van der Marel & Cioni (2001) which allow us to perform the conversion from right ascension and declination to Cartesian coordinates using a zenithal equidistant projection. We adopted the SMC optical center given by Crowl et al. (2001), $\alpha = 00^h 52^m 45^s$ and $\delta = 72^\circ 49' 43''$ [J2000.0] and the usual astronomical convention that position angle is 0 to the north and increases to the east. We have also included in the graph the seven clusters from DH98 (open circles).

Applying to our sample the maximum likelihood method (explained, for example, in the appendix B of Hargreaves et al. 1994), we have calculated a mean heliocentric velocity of $148 \pm 6 \text{ km s}^{-1}$ and a velocity dispersion of $23.6^{+5.7}_{-3.3} \text{ km s}^{-1}$, in agreement with the DH98 cluster results. When we include in the calculation the DH98 clusters, the mean heliocentric velocity and the velocity dispersion are 145 ± 5 and $22.3^{+4.2}_{-2.6} \text{ km s}^{-1}$ respectively. These values compare well with previously derived values, suggesting that the star cluster system shares the same kinematics as other tracers in the SMC.

The distribution of the points in Figure 15 may hint at rotation with a maximum at position angle of ~ 90 degrees and an amplitude of perhaps 20 km s^{-1} . However, this result is not statistically significant, as the fitting of the points (curve in Figure 15) is not statistically better than a straight line. If any apparent rotation is indeed present, we must agree with Harris & Zaritsky (2006) that this could be due to projected tangential motion and that any possible rotation velocity is smaller than the velocity dispersion.

9. Summary and Conclusions

Magellanic Cloud clusters are an excellent laboratory for helping to unlock the secrets of cluster and galaxy formation. They are also crucial testbeds for stellar and chemical evolution models and interpreting the integrated light of distant galaxies. However, despite their utility and proximity, Small Magellanic Cloud clusters in particular have been overlooked in this regard. In order to help remedy this situation, we have carried out a large-scale investigation of the kinematics and metallicities for a number of SMC star clusters. Building on our experience with deriving these parameters for LMC clusters using the CaT technique (G06), we have used the same technique to explore SMC clusters. We obtained CaT spectra for a number of stars associated with 16 SMC clusters using the VLT + FORS2 MXU instrument. This provides the largest sample of SMC clusters with velocities and well-determined spectroscopic metallicities currently available, more than doubling the only previous study (DH98). Target clusters were selected from our Washington photometric system studies, which provide a rough estimate of age and abundance, to be old enough to possess red giant branch stars and cover a wide area across the galaxy.

We used the same reduction and analysis techniques as we did in G06 to measure stellar radial velocities and metallicity. Typical radial velocities errors are 7.5 km s^{-1} and metallicity errors are 0.17 dex per star. Cluster members are selected using an analysis combining their location in the CMD, position in the cluster, and radial velocities and metallicity with respect to other stars in the same field. We determine mean cluster velocities to typically 2.7 km s^{-1} and metallicities to 0.05 dex (random error), from a mean of 6.4 members per cluster. A comparison of our mean cluster metallicities with those derived from Washington photometry for 11 clusters in common shows very good overall agreement, with the CaT metallicities being much more precise. This indicates that the

Washington metallicities, and especially their procedure used to correct the age dependence of their metallicities for their age dependence, is appropriate.

The metallicity distribution (MD), metallicity gradient and age-metallicity relation (AMR) are investigated, combining our clusters with those observed by DH98 and Glatt et al. (also with CaT) and the one cluster with a detailed, high resolution metallicity to compile a sample of 25 clusters on a homogenous metallicity scale with relatively small errors, although the ages are somewhat heterogeneous. The mean metallicity is $[\text{Fe}/\text{H}] = -0.96$, with $\sigma = 0.19$. Dividing the sample into two age groups at 3 Gyr, the 12 older clusters have a mean metallicity of -1.08 , $\sigma = 0.17$, while the 13 younger have -0.85 , 0.15 . Most clusters lie between $[\text{Fe}/\text{H}] = -0.75$ and -1.25 . There is a suggestion for bimodality in the MD, with peaks at $[\text{Fe}/\text{H}] \sim -0.9$ and -1.15 . No clear gradient is seen with distance from the center of the SMC. However, intermediate-age SMC clusters are both significantly more metal-poor and have a larger metallicity spread than their LMC counterparts. The AMR shows evidence for 3 phases: a very early (> 11 Gyr) phase in which the metallicity reached ~ -1.2 , a long intermediate phase from $\sim 10 - 3$ Gyr in which the metallicity only slightly increased although a number of clusters formed, and a final phase from 3-1 Gyr ago in which the rate of enrichment was substantially faster. These salient features agree with those found by most other AMR studies using other tracers and techniques. We find good overall agreement with the model of PT98 which assumes a burst of star formation at 4 Gyr. A hybrid infall + outflow model of Carrera (2005) also fits the data reasonably well. The simple closed box model of DH98 yields a much poorer fit, and the AMRs derived by Harris & Zaritsky (2004) and Idiart et al. (2007) are significantly offset to higher metallicities for intermediate-age clusters. A number of different lines of evidence point to the likelihood of a burst in the SMC star and cluster formation about 3 Gyr ago. The cause of such a burst is currently a source of much speculation. The suggestion by Bekki et al. (2004) that it is due to a close passage of the SMC and LMC is intriguing but requires

better knowledge of their orbits, especially proper motions, to be definitively tested.

We finally examine the kinematics of our CaT clusters. Their mean radial velocity is $= 148 \text{ km s}^{-1}$, with a velocity dispersion of 23.6 km s^{-1} . These values are in very good agreement with those found by DH98 from their smaller sample. Combining the 2 cluster samples, we find the kinematics are dominated by the velocity dispersion, as found in virtually all other kinematic studies of a wide variety of SMC populations.

This work is based on observations collected at the European Southern Observatory, Chile, under program number 076.B-0533. We would like to thank the Paranal Science Operations Staff. We would like to thank to the referee for comments that helped to improve this work. D.G. gratefully acknowledges support from the Chilean Centro de Astrofísica FONDAF No. 15010003 and the Chilean Centro de Excelencia en Astrofísica y Tecnologías Afines (CATA). M.C.P. acknowledges Andrew Cole and Andrés Piatti for their explanations and discussion about how to perform some calculations and Ricardo Carrera for allowing us to use his unpublished age-metallicity models. M.C.P. and J.J.C. gratefully acknowledge financial support from the Argentinian institutions CONICET and SECYT (Universidad Nacional de Córdoba).

Facilities: VLT: Antu (FORS2).

REFERENCES

- Armandroff, T.E., & Da Costa, G.S. 1991, *AJ*, 101, 1329
- Armandroff, T.E., & Zinn, R. 1988, *AJ*, 96, 92
- Ashman, K.M., Bird, C.M., & Zepf, S.E. 1994, *AJ*, 108, 2348
- Bastian, N., Gieles, M., Ercolano, B., & Gutermuth, R. 2009, *MNRAS*, 392, 868
- Battaglia, G., Helmi, A., Tolstoy, E., & Irwin, M.J. 2007, *ASPC*, 374, 273
- Bekki, K., Couch, W.J., Beasley, M.A., Forbes, D.A., Chiba, M., & Da Costa, G.S. 2004, *ApJ*, 610, L93
- Bica, E., Dottori, H., & Pastoriza, M.G. 1986, *A&A*, 156, 261
- Carrera, R. 2005, Ph. D. Thesis, Departamento de Astrofísica, Universidad de La Laguna, España.
- Carrera, R., Gallart, C., Aparicio, A., Costa, E., Méndez, R.A., & Noël, N.E.D. 2008, *AJ*, 136, 1039
- Carrera, R., Gallart, C., Pancino, E., & Zinn, R. 2007, *AJ*, 134, 1298
- Carretta, E., & Gratton, R.G. 1997, *A&AS*, 121, 95
- Cenarro, A.J., Gorgas, J., Cardiel, N., Vazdekis, A., & Peletier, R.F. 2002, *MNRAS*, 329, 863
- Chandar, R., Fall, S.M., & Whitmore, B.C. 2006, *ApJ*, 650, 111
- Cole, A.A., Smecker-Hane, T.A., & Gallagher J.S. III 2000, *AJ*, 120, 1808

- Cole, A.A., Smecker-Hane, T.A., Tolstoy, E., Bosler, T.L., & Gallagher, J.S. 2004, MNRAS, 347, 367 (C04)
- Crowl, H.H., Sarajedini, A., Piatti, A.E., Geisler, D., Bica, E., Clariá, J.J., & Santos, J.F.C. Jr. 2001, AJ, 122, 220
- Da Costa, G.S. 1991, in IAU Symp. 148, The Magellanic Clouds, ed. R. Haynes & D. Milne (Dordrecht: Kluwer), 183
- Da Costa, G.S., & Hatzidimitriou, D. 1998, AJ, 115, 1934 (DH98)
- Dopita, M.A. 1991, in IAU Symp. 148, The Magellanic Clouds, ed. R. Haynes & D. Milne (Dordrecht: Kluwer), 393
- Dopita, M.A., Lawrence, C.J., Ford, H.C., & Webster, B.L. 1985, ApJ, 296, 390
- Friel, E.D., Janes, K.A., Tavares, M., Scott, J., Katsanis, R., Lotz, J., Hong, L., & Miller, N. 2002, AJ, 124, 2693
- Gardiner, L.T., Sawa, T., & Fujimoto, M. 1994, MNRAS, 266, 567
- Geisler, D., Bica, E., Dottori, H., Clariá, J.J., Piatti, A.E., & Santos, J.F.C. Jr. 1997, AJ 114, 1920
- Geisler, D., Piatti, A.E., Bica, E., & Clariá, J.J. 2003, MNRAS, 341, 771
- Geisler, D., & Sarajedini, A. 1999, AJ, 117, 308
- Geisler, D., Wallerstein, G., Smith, V.V., & Casetti-Dinescu, D.I. 2007, PASP, 119, 939
- Glatt, K., et al. 2008a, AJ, 135, 1106
- Glatt, K., et al 2008b, AJ, 136, 1703
- Gonzalez, G., & Wallerstein, G. 1999, AJ, 117, 2286

- Grocholski, A.J., Cole, A.A, Sarajedini, A., Geisler, D., & Smith, V. 2006, AJ, 132, 1630
(G06)
- Hardy, E., Suntzeff, N.B., & Azzopardi, M. 1989, ApJ, 344, 210
- Hargreaves, J. C., Gilmore, G., Irwin, M. J. & Carter, D., 1994, MNRAS, 269, 957
- Harris, J., & Zaritsky, D. 2004, AJ, 127, 1531
- Harris, J., & Zaritsky, D. 2006, AJ, 131, 2514
- Hatzidimitriou, D., Cannon, R.D., & Hawkins, M.R.S. 1993, MNRAS, 261, 873
- Hatzidimitriou, D., Croke, B.F., Morgan, D.H., & Cannon, R.D. 1997, A&AS, 122, 507
- Hill, V. 1997, A&A, 324, 435
- Hill, V. 1999, A&A, 345, 430
- Hodge, P. 1986, PASP, 98, 1113
- Idiart, T.P., Maciel, W.J., & Costa, R.D.D. 2007, A&A, 472, 101
- Irwin, M., & Tolstoy, E. 2002, MNRAS, 336, 643
- Janes, K.A. 1979, ApJS, 39, 135
- Johnson, J.A., Bolte, M., Hesser, J.E., Ivans, I.I., & Stetson, P.B. 2004, Carnegie
Observatories Astrophysics Ser. 4, ed. A. McWilliam & M. Rauch, p.29
- Jørgensen, U.G., Carlsson, M., & Johnson, H.R. 1992, A&A, 254,258
- Kallivayalil, N., van del Marel, R.P., & Alcock, C. 2006, ApJ, 652, 1213
- Kayser, A., Grebel, E.K., Harbeck, D.R., Cole, A.A., Koch, A., Gallagher, J.S., & Da
Costa, G.S. 2006, preprint (astro-ph/0607047)

- Lada, C.J., & Lada, E.A. 2003, *ARA&A*, 41, 57
- Mathewson, D.S., Ford, V.L., & Visvanathan, N. 1988, *ApJ*, 333, 617
- Maurice, E., et al. 1987, *A&AS*, 67, 423
- McCumber, M., Garnett, D.R., & Dufour, R.J. 2005, *AJ*, 130, 1083
- Murai, T., & Fujimoto, M. 1980, *PASJ*, 32, 581
- Noël, N.E.D., Gallart, C., Aparicio, A., Hidalgo, S., Carrera, R., Costa, E. & Méndez, R.A. 2007, in *Symp. 241, Stellar Populations as Building Blocks of Galaxies*, ed. A. Vazdekis and R. F. Peletier, (Cambridge: CUP), 305
- Olszewski, E.W., Schommer, R.A., Suntzeff, N.B., & Harris, H.C. 1991, *AJ*, 101, 515
- Olszewski, E.W., Suntzeff, N.B., & Mateo, M. 1996, *ARA&A*, 34, 511
- Pagel, B.E.J., & Tautvaišienė, G. 1998, *MNRAS*, 299, 535 (PT98)
- Piatek, S., Pryor, C., & Olszewski, E.W. 2008, *AJ*, 135, 1024
- Piatti, A.E., Santos, J.F.C. Jr., Clariá, J.J., Bica, E., Ahumada, A.V., & Parisi, M.C. 2005b, *A&A*, 440, 111
- Piatti, A.E., Santos, J.F.C. Jr., Clariá, J.J., Bica, E., Sarajedini, A., & Geisler, D. 2001, *MNRAS*, 325, 792
- Piatti, A.E., Sarajedini, A., Geisler, D., Clark, D., & Seguel, J. 2007a, *MNRAS*, 377, 300
- Piatti, A.E., Sarajedini, A., Geisler, D., Gallart, C., & Wischnjewsky, M. 2007b, *MNRAS*, 381, L84
- Piatti, A.E., Sarajedini, A., Geisler, D., Gallart, C., & Wischnjewsky, M. 2007c, *MNRAS*, 382, 1203

- Piatti, A.E., Sarajedini, A., Geisler, D., Seguel, J., & Clark, D. 2005a, MNRAS, 358, 1215
- Pietrinferni, A., Cassisi, S., Salaris, M., & Castelli, F. 2004, ApJ, 612, 168
- Pryor, C., & Meylan, G. 1993, Structure and Dynamics of Globular Clusters, ASP Conf. Ser. 50, p. 357
- Rafelski, M., & Zaritsky, D. 2005, AJ, 129, 2701
- Rich, R.M., Shara, M., Fall, S.M., & Zurek, D. 2000, AJ, 119, 197
- Robertson, B., Bullock, J.S., Font, A.S., Johnston, K.V., & Hernquist, L. 2005, ApJ, 632, 872
- Russell, S.C., & Bessell, M.S. 1989, ApJS, 70, 865
- Rutledge, G.A., Hesser, J.E., & Stetson, P.B. 1997a, PASP, 109, 907
- Rutledge, G.A., Hesser, J.E., Stetson, P.B., Mateo, M., Simard, L., Bolte, M., Friel, E.D., & Copin, Y. 1997b, PASP, 109, 883
- Searle, L., & Zinn, R. 1978, ApJ, 225, 357
- Shetrone, M.D., Côté, P., & Sargent, W.L.W. 2001, ApJ, 548, 592
- Stanimirović, S., Staveley-Smith, L., & Jones, P.A. 2004, ApJ, 604, 176
- Staveley-Smith, L., Sault, R.J., Hatzidimitriou, D., Kesteven, M.J., & McConnell, D. 1997, MNRAS, 289, 225
- Stetson, P.B. 1987, PASP, 99, 191
- Stryker, L.L., Da Costa, G.S., & Mould, J.R. 1985, ApJ, 298, 544
- Suntzeff, N.B., Friel, E., Klemola, A., Kraft, R.P., & Graham, J.A. 1986, AJ, 91, 275

Suntzeff, N.B., Mateo, M., Terndrup, D.M., Olszewski, E.W., Geisler, D., & Weller, W.
1993, ApJ, 418, 208

Tonry, J., & Davis, M. 1979, AJ, 84, 1511

Tsujimoto, T., Nomoto, K., Yoshii, Y., Hashimoto, M., Yanagida, S., & Thielemann, F.-K.
1995, MNRAS, 277, 945

van der Marel, R.P., & Cionni, M.-R.L. 2001, AJ, 122, 1807

Yoshizawa, A. M., & Noguchi, M. 2003, MNRAS, 339, 1135

Zaritsky, D., Harris, J., Thompson, I.B., Grebel, E.K., & Massey, P. 2002, AJ, 123, 855

Zaritsky, D., Kennicutt, R.C., Jr., & Huchra, J.P. 1994, ApJ, 420, 87

Zentner, A.R., & Bullock, J.S. 2003, ApJ, 598, 49

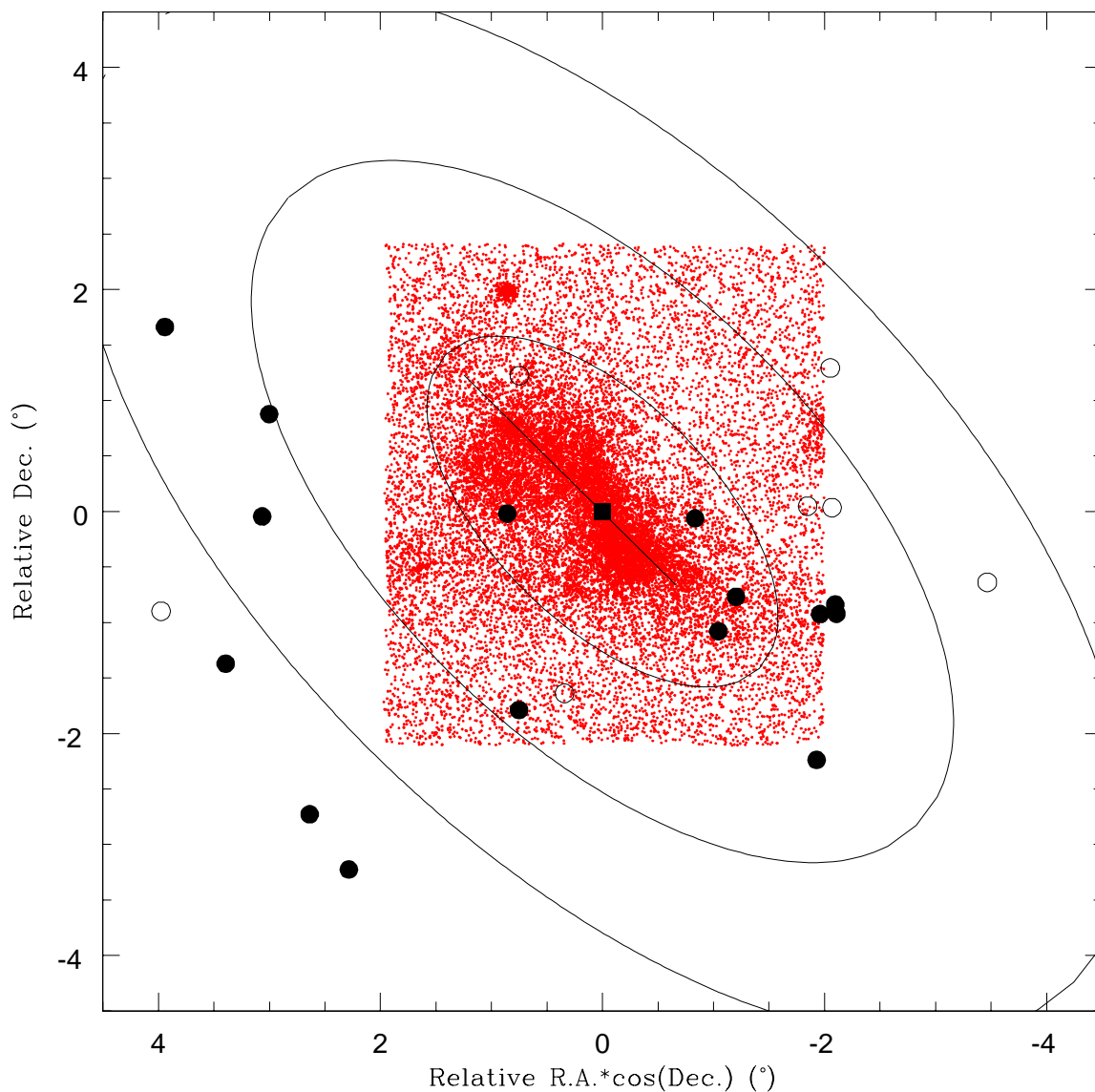


Fig. 1.— Position of our target clusters (filled circles) in relation to the SMC optical centre (square) and the SMC bar (line). Open circles represent the position of clusters from DH98. The ellipses are aligned with the bar and have semi-major axis of 2, 4 and 6 degrees. Following the idea of Glatt et al. (2008b), a star map of the SMC is superposed. This map was generated by using the catalog of the Small Magellanic Cloud Photometric Survey (Zaritsky et al. 2002) for stars with $V < 16$.

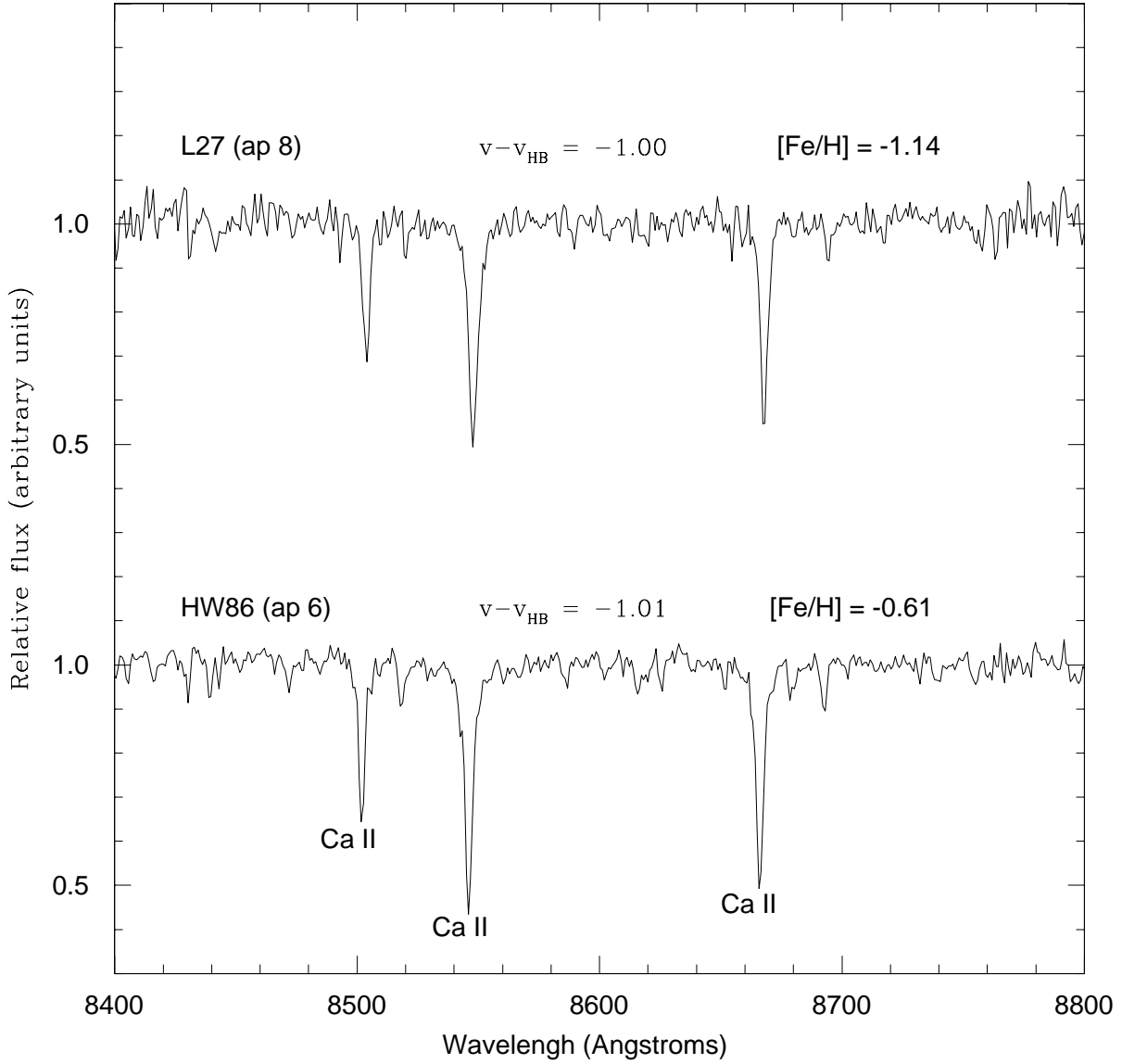


Fig. 2.— Sample continuum-normalised spectra of RGB stars in two clusters of our sample. The three CaT lines have been marked on the plot as well as the corresponding $v - v_{HB}$ values and metallicities. These 2 stars have very similar T_{effs} and $\log g$ values. Thus, the clear difference in Ca II line strength illustrates their substantial metallicity difference.

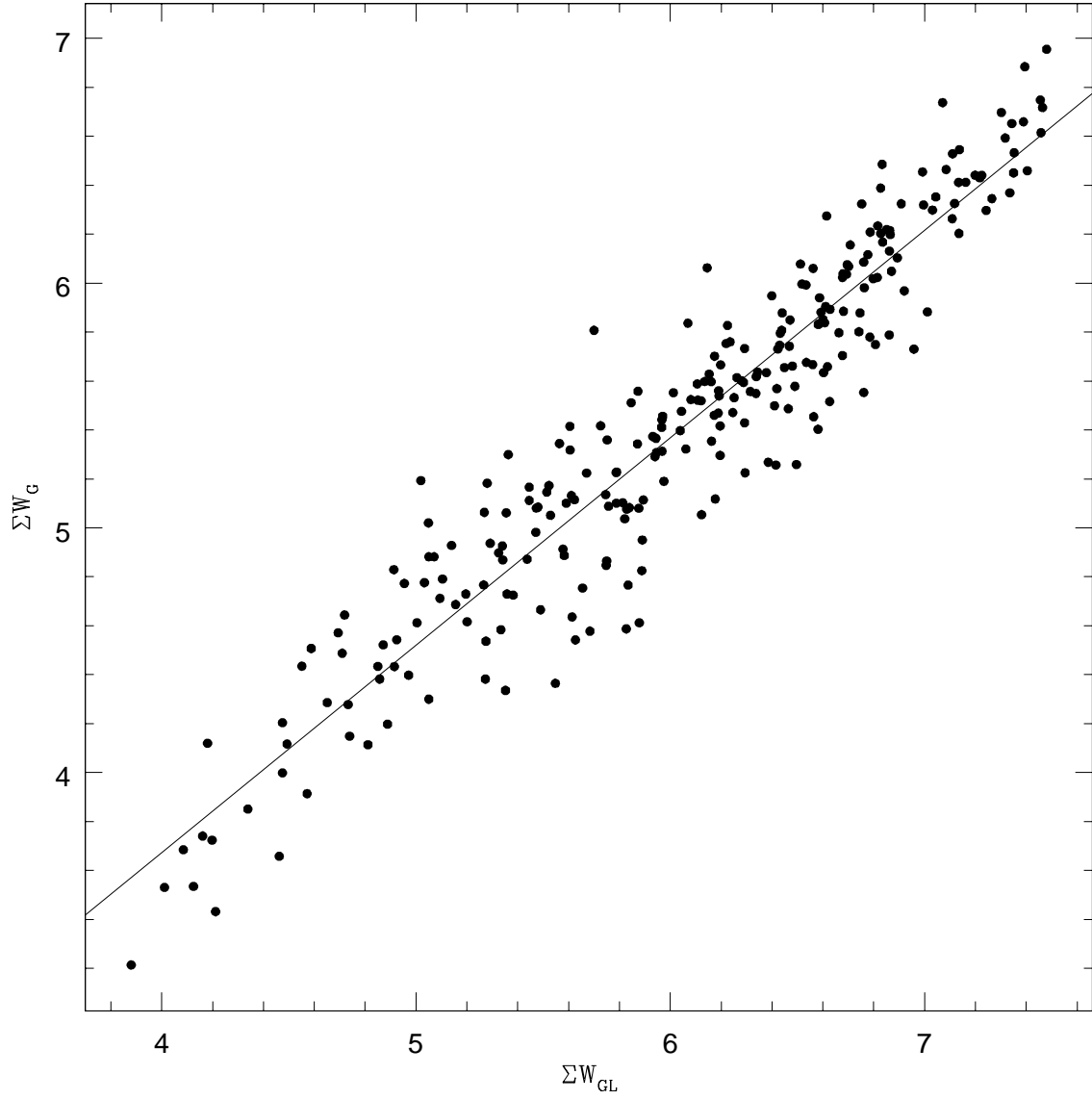


Fig. 3.— Relation between the Gaussian-fit EW, ΣW_G , and the Gaussian + Lorentzian-fit, ΣW_{GL} . The points correspond to spectra with $S/N > 20$ and the solid line shows the linear fit to the data.

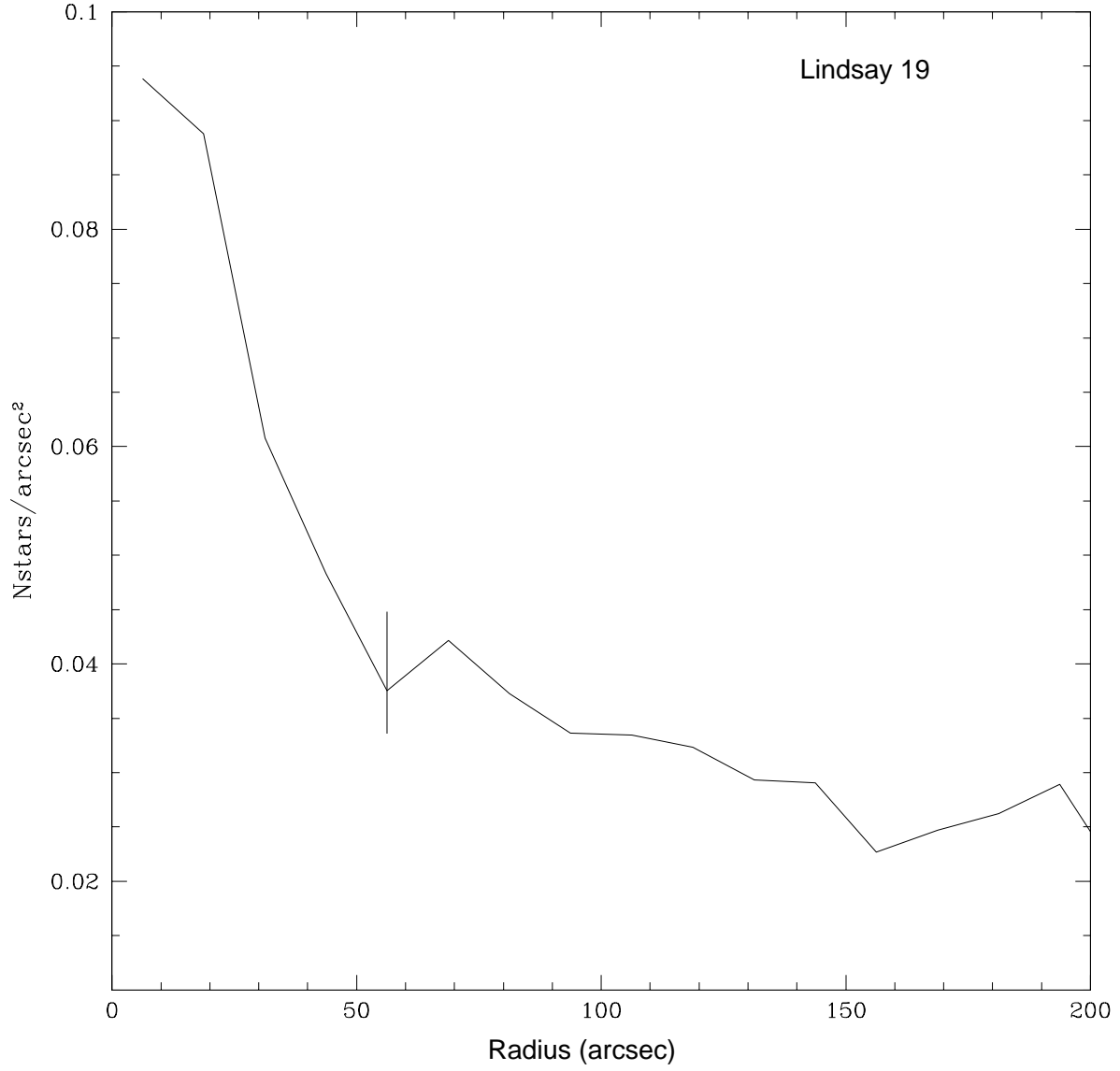


Fig. 4.— Radial stellar density profile of the cluster Lindsay 19. The x-axis represents the radius and the y-axis represents the stellar number density. The adopted cluster radius is marked.

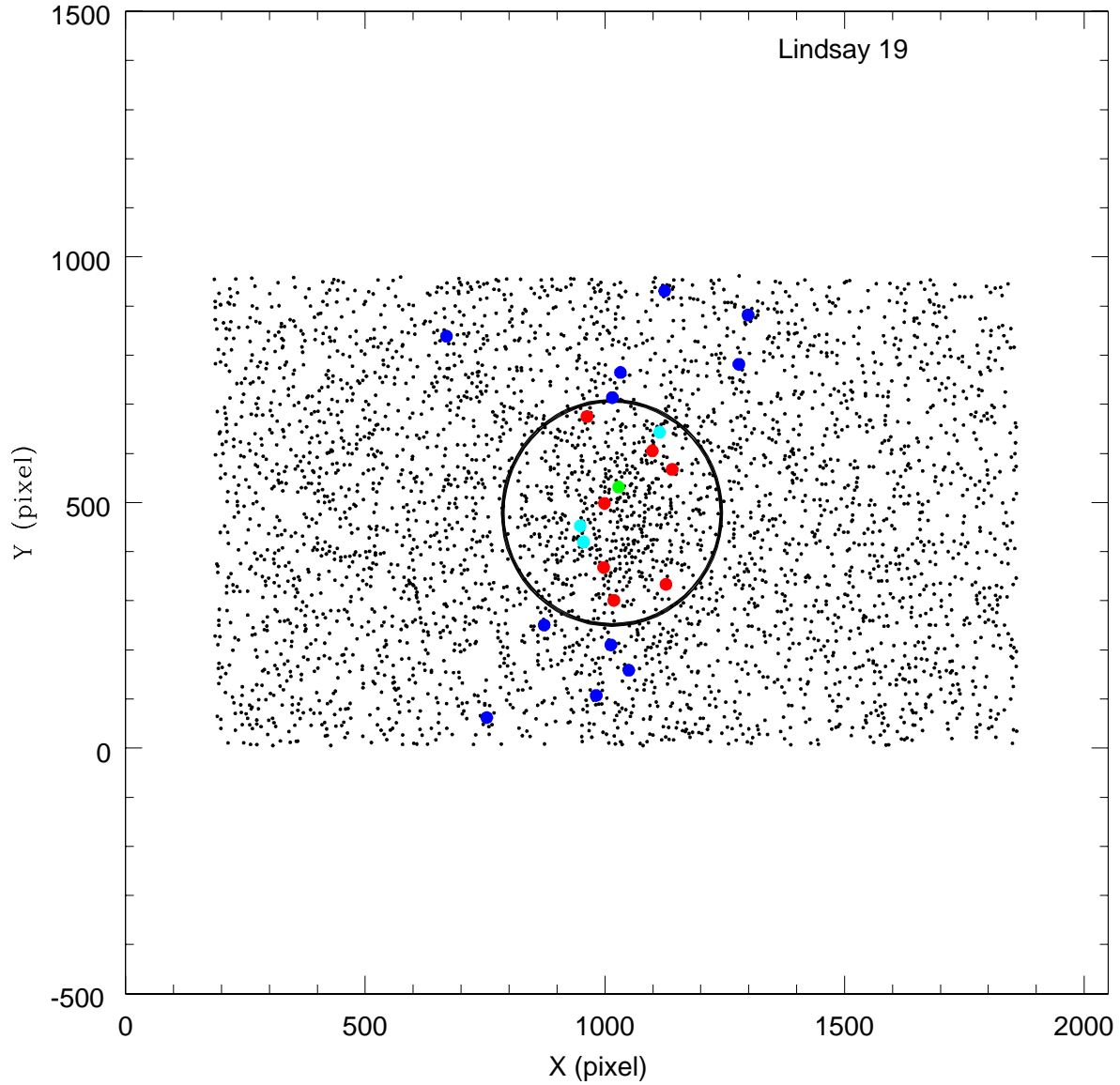


Fig. 5.— Chart of the cluster Lindsay 19. Our spectroscopic target stars are represented by the large filled circles and the adopted cluster radius is represented by a large circle. Color code: non-members that are outside the cluster radius (blue circles), non-members that were eliminated because of discrepant radial velocity or metallicity (teal and green circles, respectively) and final cluster members (red circles).

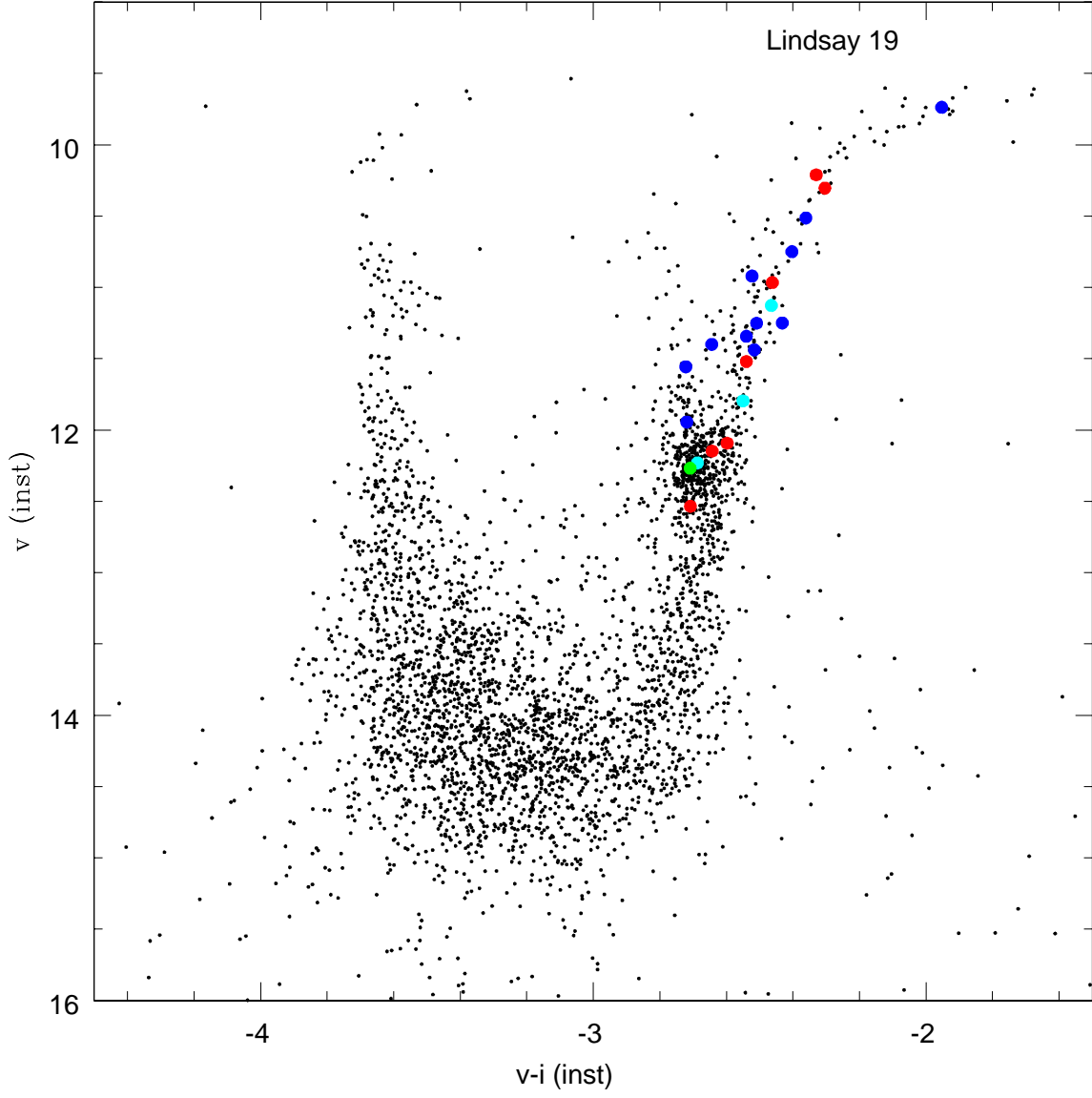


Fig. 6.— Instrumental color-magnitude diagram of Lindsay 19. The color code is the same as in Figure 5.

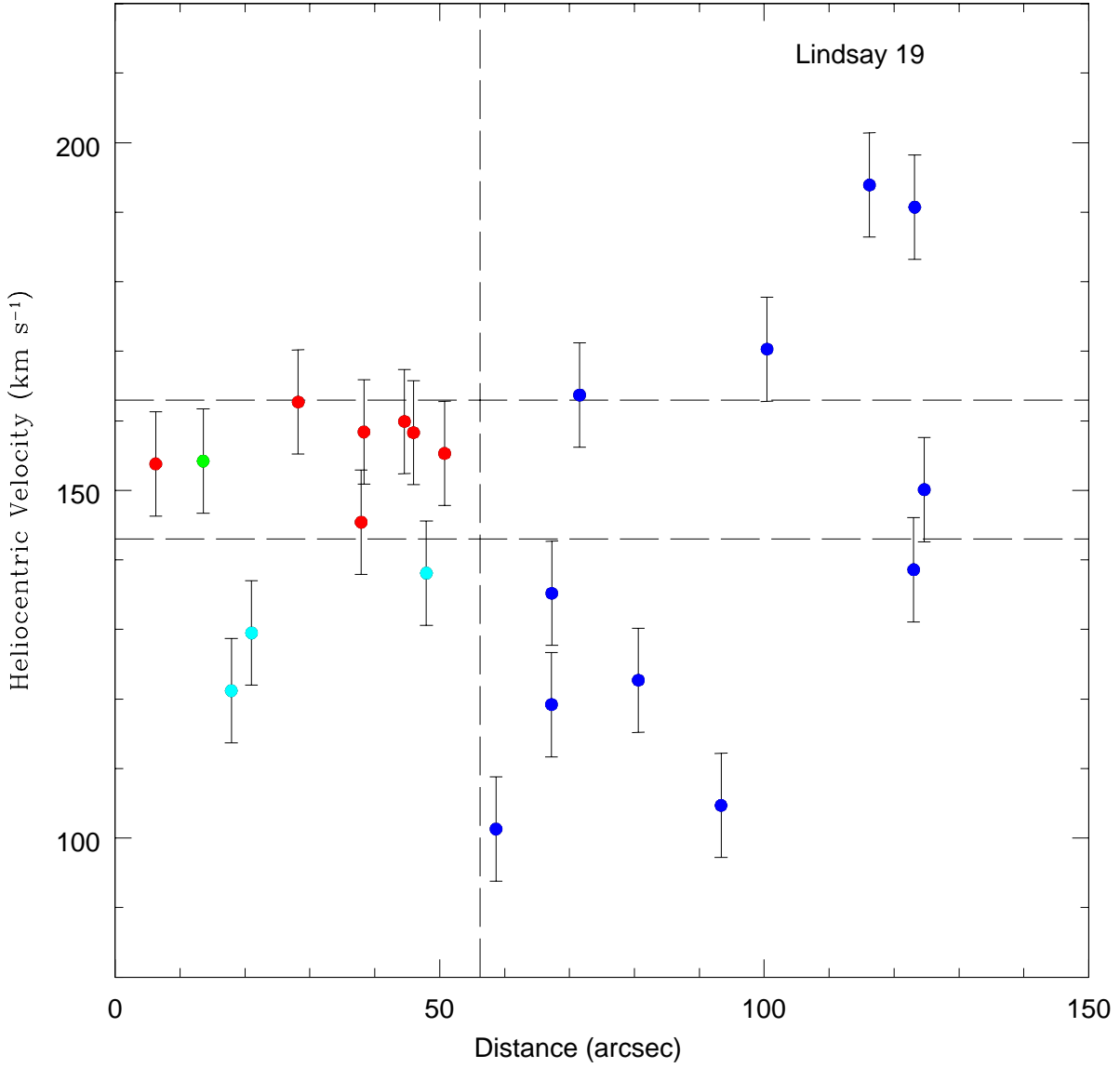


Fig. 7.— Radial velocity vs. distance from the cluster center for Lindsay 19 targets. The horizontal lines represent our velocity error cut ($\pm 10 \text{ km s}^{-1}$) and the vertical line represents the adopted cluster radius. The color code is the same as in Figure 5. Error bars represent the random error in determining the RV for each star.

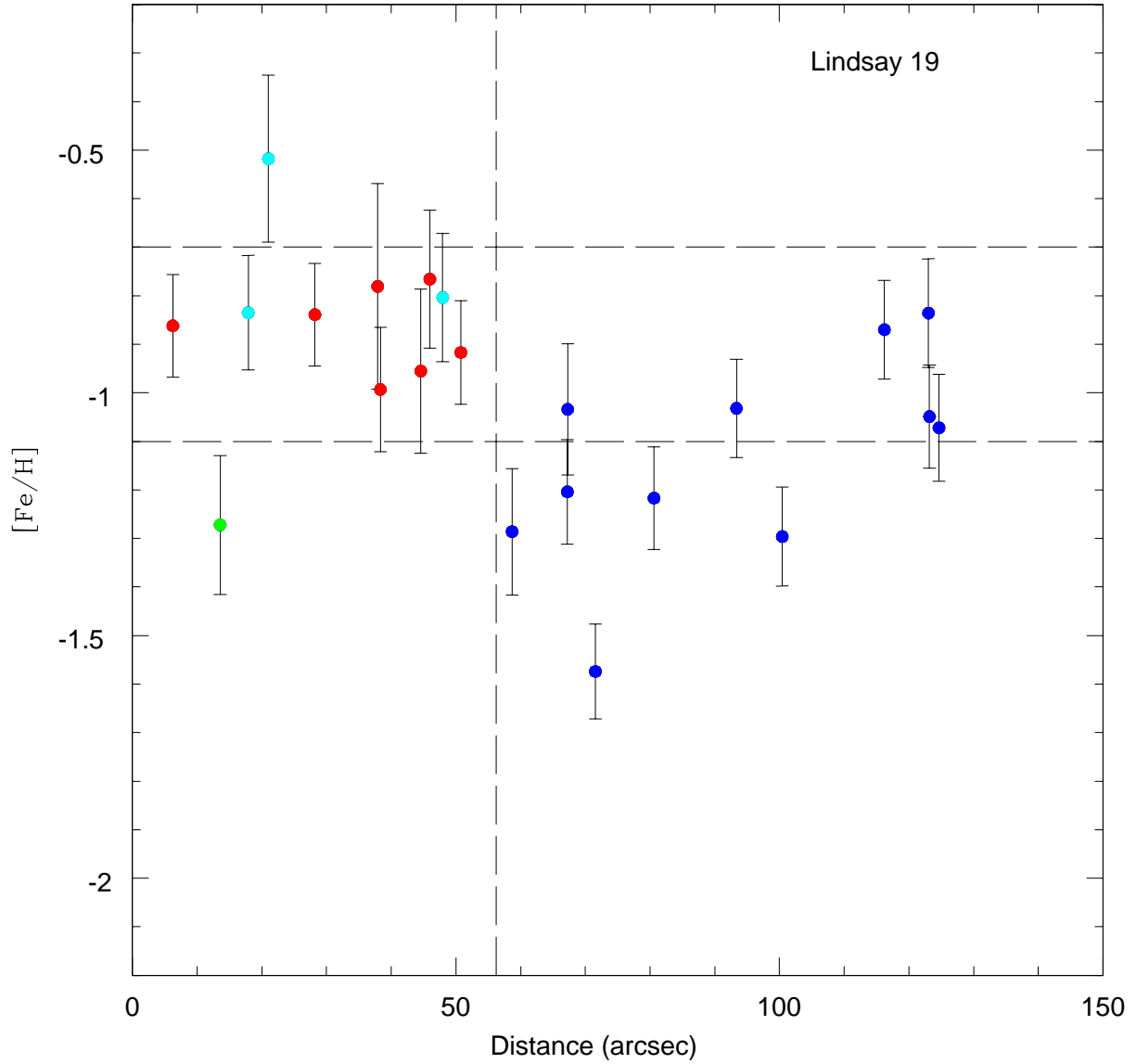


Fig. 8.— Metallicity versus distance from the cluster center for Lindsay 19 targets. Horizontal lines represent the $[Fe/H]$ error cut (± 0.20 dex) and the vertical line represents the adopted cluster radius. The color code is the same as in Figure 5. Error bars represent the random error in calculating $[Fe/H]$.

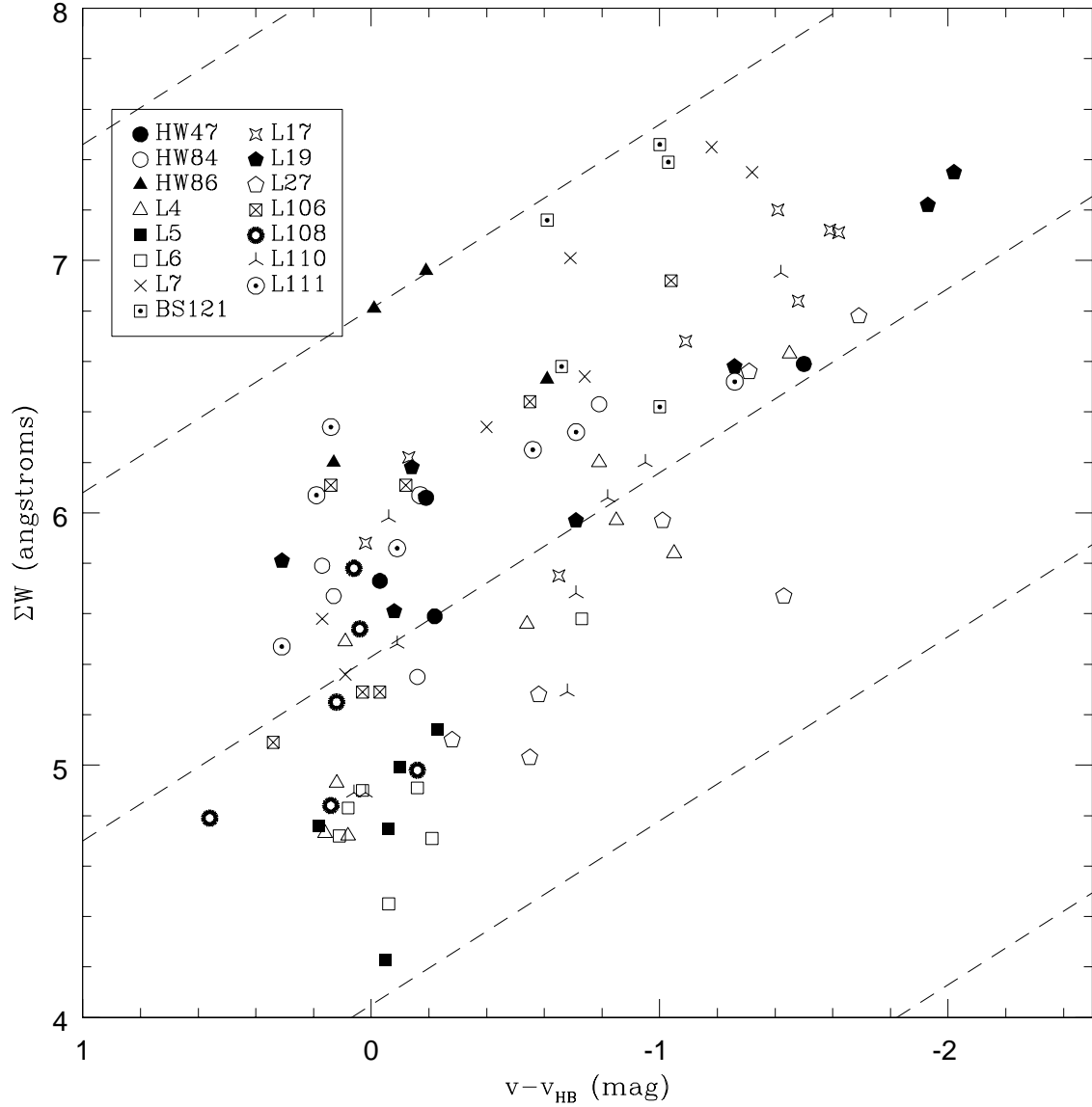


Fig. 9.— The sum of the equivalent width of the three CaT lines versus $v - v_{HB}$ for identified members of all clusters. The dashed lines represent isometallicity lines of 0, -0.5, -1, -1.5 and -2 (from top to bottom).

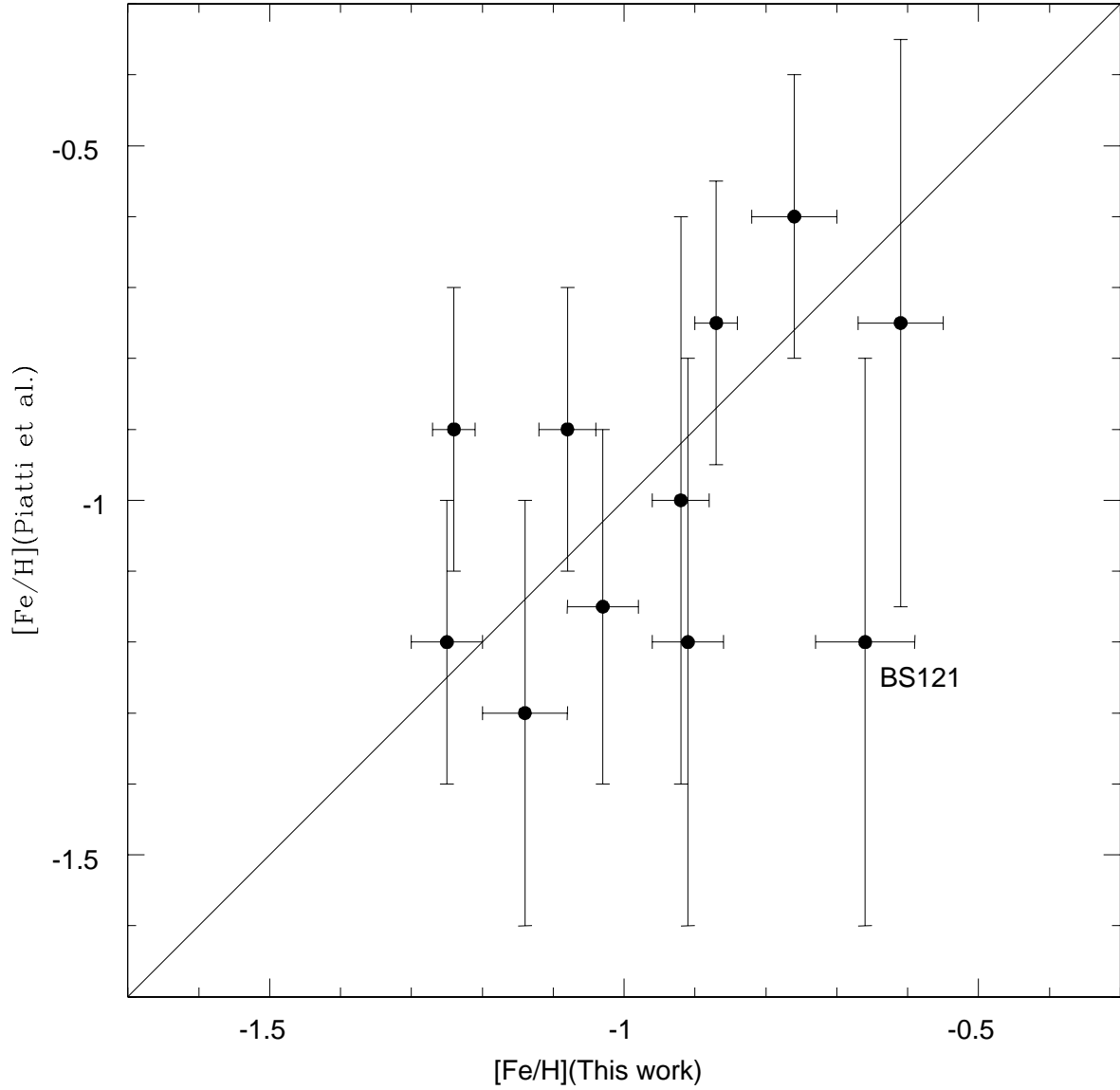


Fig. 10.— Comparison of our spectroscopic mean cluster metallicities and those derived from Washington photometry by Piatti et al. (2005a, 2007b). The line shows one-to-one correspondence. Note that there is no systematic difference between the two systems but that the error of the CaT technique is substantially smaller. The only cluster showing a considerable difference between both metallicity determinations, BS 121, is marked.

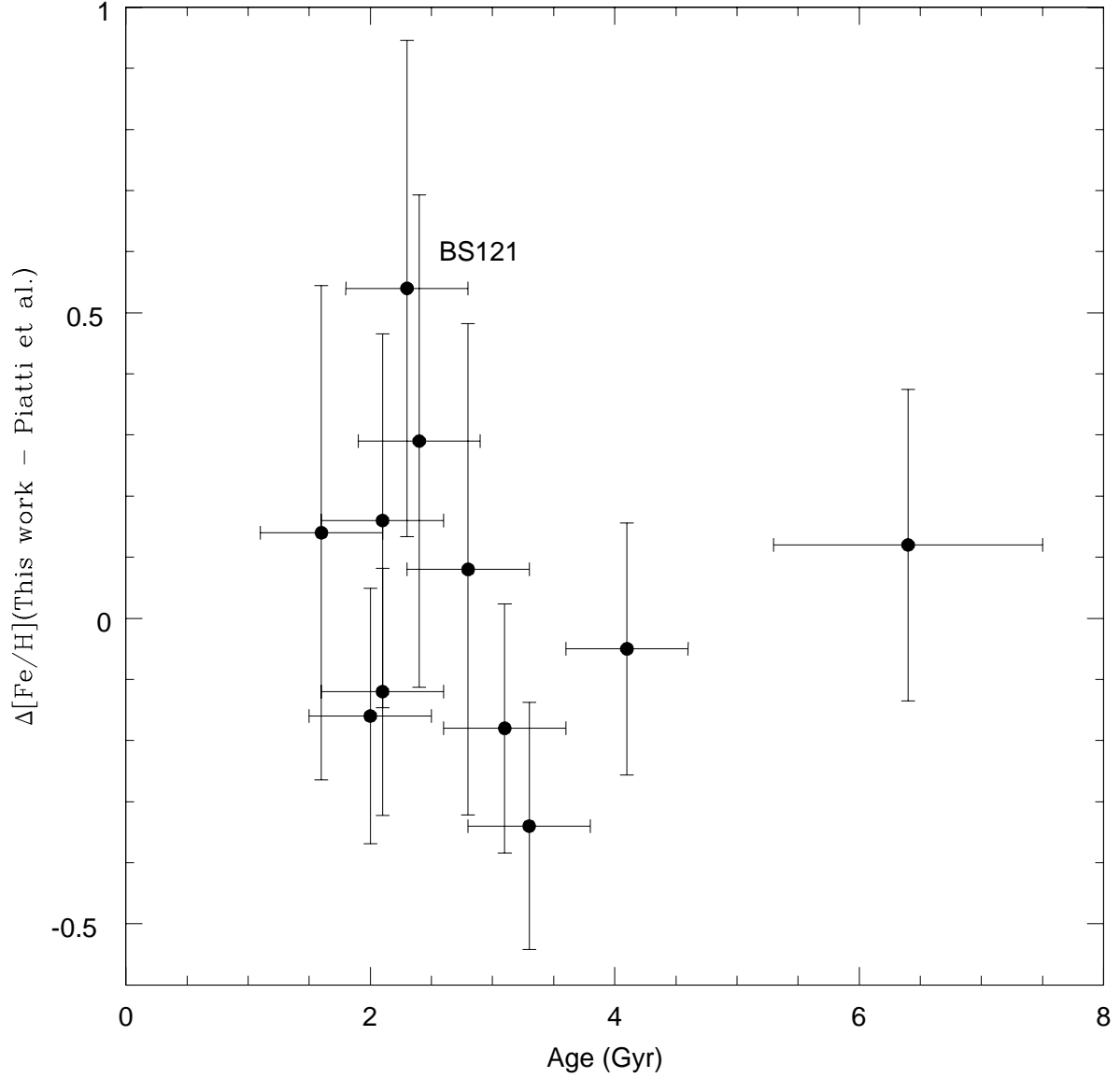


Fig. 11.— Difference between our spectroscopic mean cluster metallicity and that derived from Washington photometry by Piatti et al. (2005a, 2007b) vs. age. No systematic trend is observed. The only cluster showing a considerable difference between both metallicity determinations, BS 121, is marked.

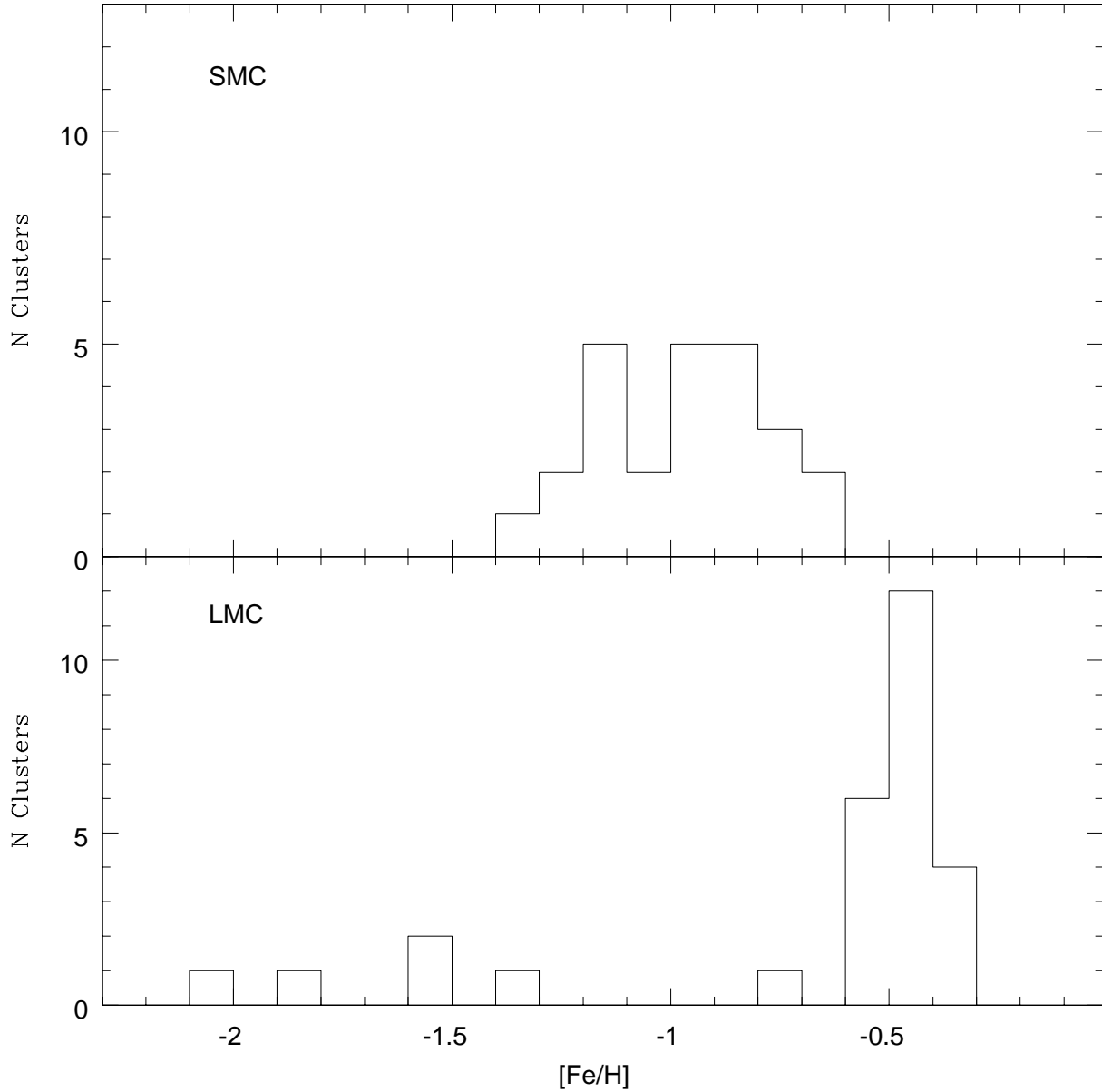


Fig. 12.— Metallicity distribution of SMC clusters (top panel): 15 from the present work, 6 from DH98, 3 from Glatt et al. (2008b) and NGC 330 (Gonzalez & Wallerstein 1999). Histogram on the bottom panel corresponds to the metallicity distribution for LMC clusters derived from our CaT investigation (G06).

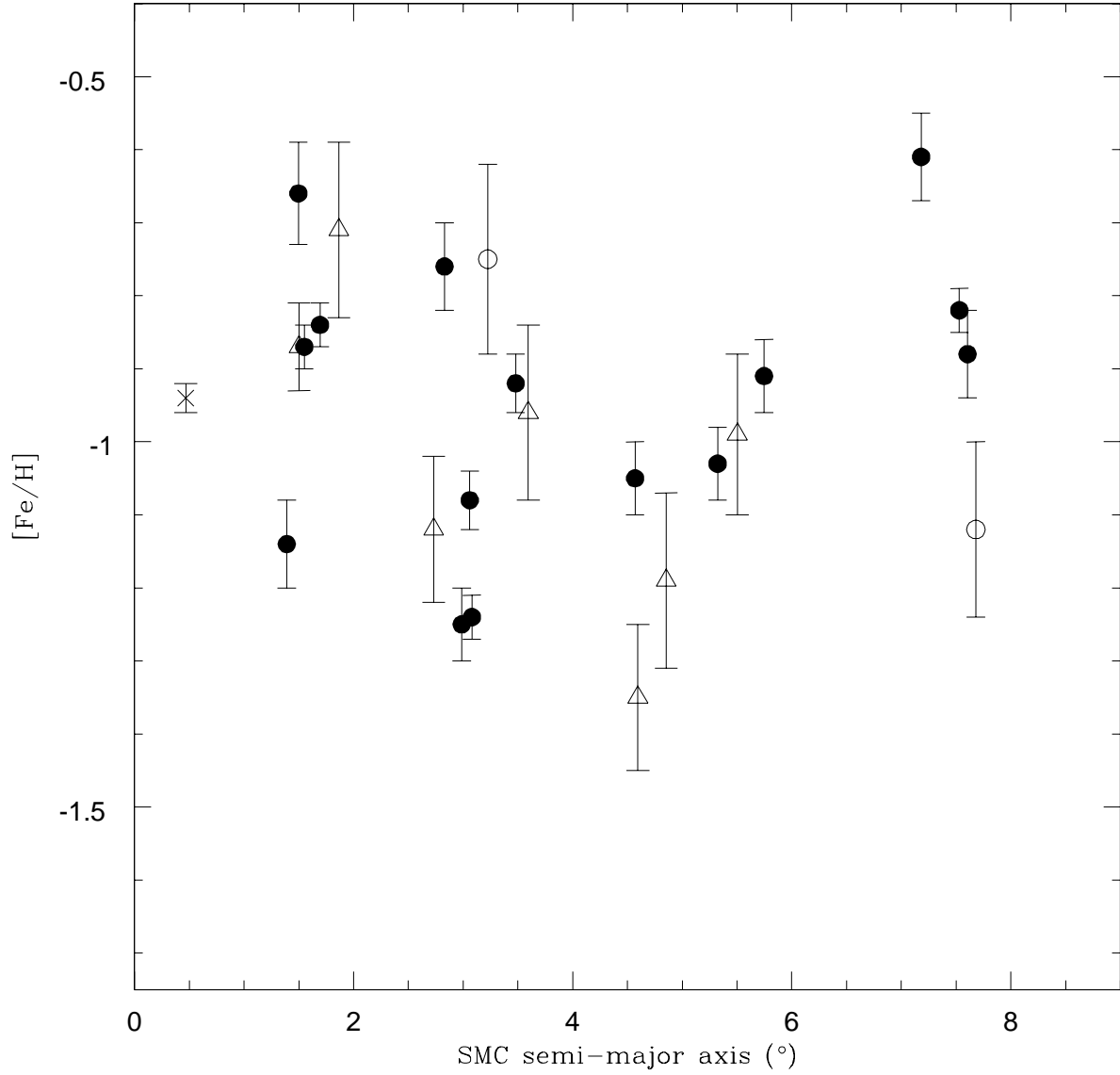


Fig. 13.— Metallicity vs. projected radius (semi-major axis a) for the SMC clusters. Open circles represent clusters from DH98 and triangles represent clusters from Glatt et al. (2008b). Clusters from our CaT sample are represented by filled circles. NGC 330 is shown by a cross. No clear trend is evident.

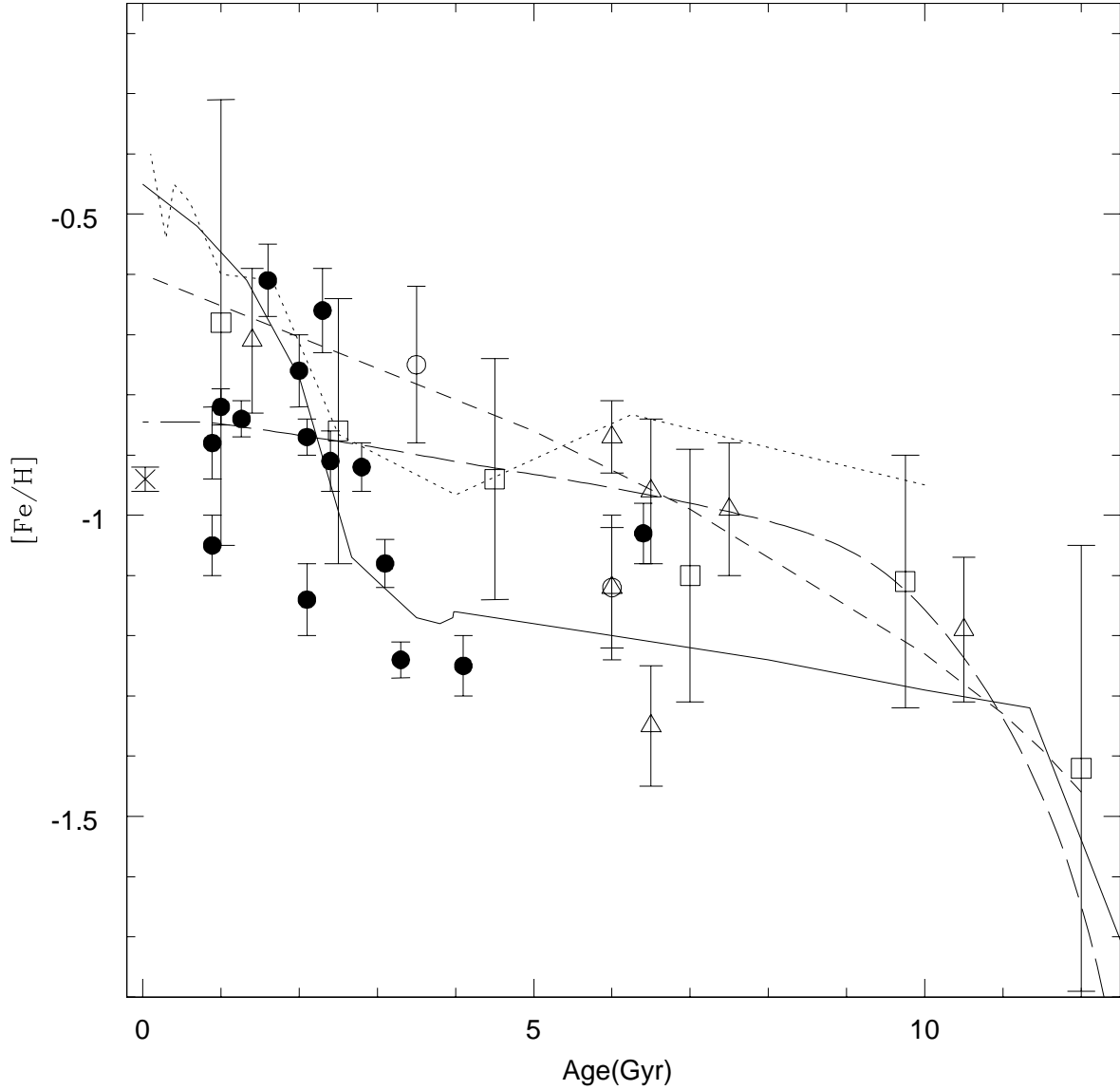


Fig. 14.— Age-Metallicity relation. Open circles represent clusters from DH98 and triangles represent clusters from Glatt et al. (2008b). Clusters of our sample are represented by filled circles. NGC 330 is shown by a cross. The mean metallicity in six age bins calculated by Carrera et al. (2008) are also shown (squares). The short dashed line represents the model of closed box continuous star formation computed by Da Costa & Hatzidimitriou (1998), the solid line corresponds to the bursting model of Pagel & Tautvaišienė (1998) and the long dashed line shows the best-fit model derived by Carrera (2005). The dotted line shows the AMR obtained by Harris & Zaritsky (2004).

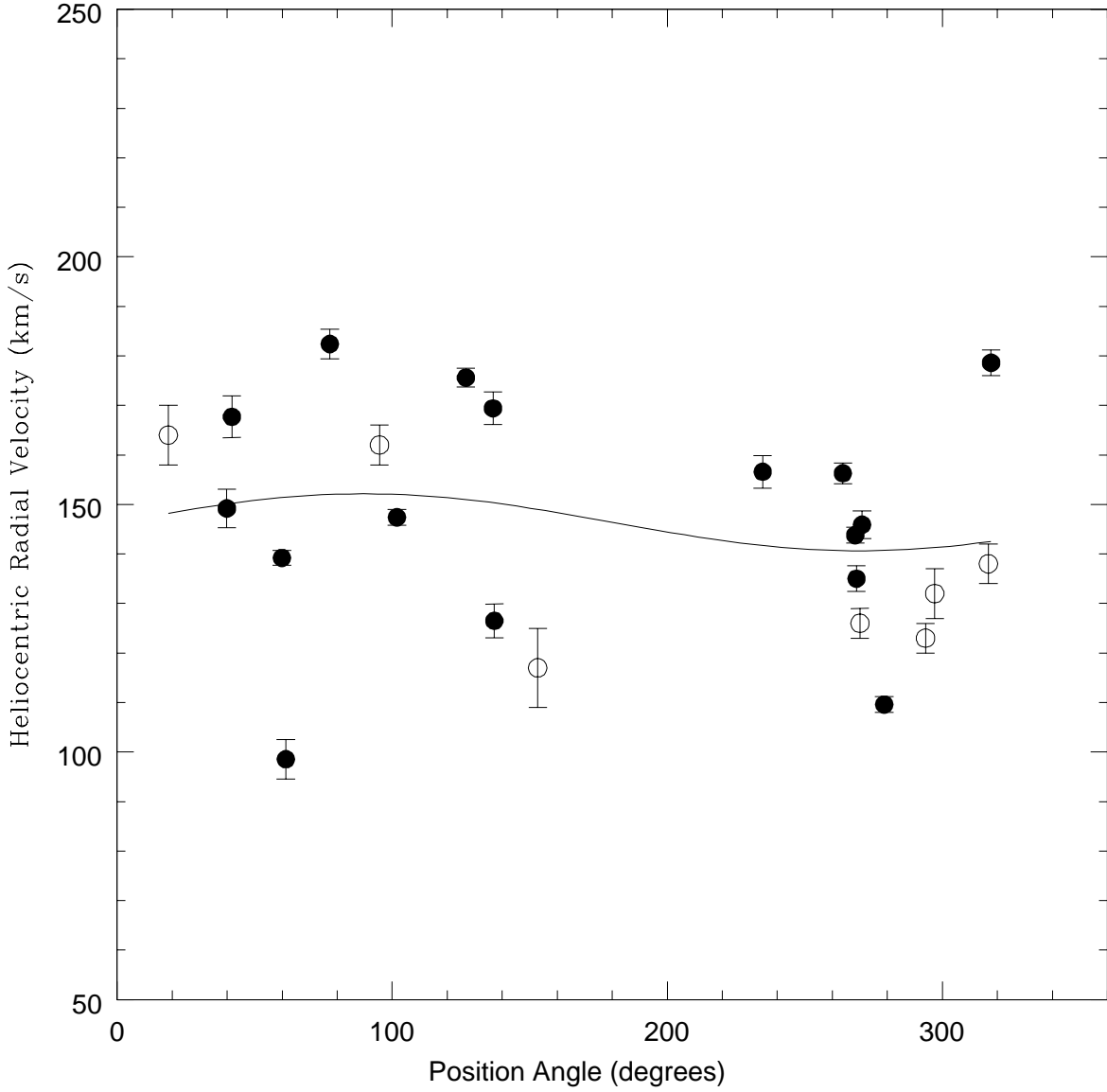


Fig. 15.— Heliocentric radial velocity as a function of position angle on the sky. Clusters from DH98 and this work are represented by open and filled circles, respectively. The solid line represents the best fit of a rotation curve. However, the curve is not statistically better than a constant velocity.

Table 1. SMC Clusters

Cluster	RA (J2000.0) (<i>h m s</i>)	Dec (J2000.0) ($^{\circ}$ <i>' "</i>)
BS 121 = SMC OGLE 237	01 04 22	-72 50 52
HW 47	01 04 04	-74 37 09
HW 84	01 41 28	-71 09 58
HW 86	01 42 22	-74 10 24
L 4 = K 1, ESO 28-15	00 21 27	-73 44 55
L 5 = ESO 28-16	00 22 40	-75 04 29
L 6 = K 4, ESO 28-17	00 23 04	-73 40 11
L 7 = K 5, ESO 28-18	00 24 43	-73 45 18
L 17 = K 13, ESO 29-1	00 35 42	-73 35 51
L 19 = SMC OGLE 3	00 37 42	-73 54 30
L 27 = K 21, SMC OGLE 12	00 41 24	-72 53 27
L 72 = NGC 376, K 49, ESO 29-29, SMC OGLE 139	01 03 53	-72 49 34
L 106 = ESO 29-44	01 30 38	-76 03 16
L 108	01 31 32	-71 57 10
L 110 = ESO 29-48	01 34 26	-72 52 28
L 111 = NGC 643, ESO 29-50	01 35 00	-75 33 24

Table 2. Position and Measured Values for Member Stars

ID	RA (J2000.0) (<i>h m s</i>)	Dec (J2000.0) ($^{\circ}$ ' ")	RV (km s^{-1})	σ_{RV} (km s^{-1})	$v-v_{HB}$ (mag)	ΣW (\AA)	$\sigma_{\Sigma W}$ (\AA)	[Fe/H]	$\sigma_{[Fe/H]}$
BS 121-2	01 04 17.53	-72 50 20.00	173.7	5.3	-0.66	6.58	0.27	-0.758	0.141
BS 121-4	01 04 21.15	-72 50 33.60	175.0	5.3	-1.00	7.46	0.17	-0.529	0.128
BS 121-5	01 04 25.85	-72 50 21.82	157.8	5.4	-1.00	6.42	0.21	-0.907	0.124
BS 121-7	01 04 24.05	-72 51 04.80	175.1	5.3	-1.03	7.39	0.15	-0.562	0.123
BS 121-12	01 04 32.46	-72 51 35.92	156.9	5.3	-0.61	7.16	0.20	-0.534	0.133

Note. — Table 2 is published in its entirety in the electronic edition of the *Astronomical Journal*. A portion is shown here for guidance regarding its form and content.

Table 3. Derived SMC Cluster Properties

Cluster	n	RV (km s ⁻¹)	σ_{RV} (km s ⁻¹)	[Fe/H] (dex)	$\sigma_{[Fe/H]}$ (dex)	P.A. (°)	a (°)
BS 121	5	167.7	4.2	-0.66	0.07	41.73	1.496
HW 47	4	126.5	3.4	-0.92	0.04	137.14	3.502
HW 84	4	139.2	1.5	-0.91	0.05	59.90	5.513
HW 86	4	147.4	1.6	-0.61	0.06	101.70	7.345
L 4	9	143.8	1.6	-1.08	0.04	268.34	3.265
L 5	5	156.6	3.3	-1.25	0.05	234.70	3.092
L 6	7	145.9	2.8	-1.24	0.03	270.81	3.124
L 7	7	135.0	2.6	-0.76	0.06	268.79	2.888
L 17	8	109.6	1.6	-0.84	0.03	278.90	1.718
L 19	7	156.3	2.1	-0.87	0.03	263.83	1.564
L 27	7	178.6	2.6	-1.14	0.06	317.73	1.392
L 72	5	149.2	3.9	39.88	1.410
L 106	7	169.4	3.3	-0.88	0.06	136.64	7.877
L 108	6	98.55	4.0	-1.05	0.05	61.37	4.460
L 110	9	182.4	3.0	-1.03	0.05	77.32	5.323
L 111	8	175.6	1.9	-0.82	0.03	126.81	7.830

Table 4. Photometric Cluster Metallicities and Ages

Cluster	Metallicity (dex)	Age (Gyr)	Reference Met., Age
BS 121	-1.2 ± 0.4	2.3	1, 1
HW 47	-1.0 ± 0.4	2.8	1, 1
HW 84	-1.2 ± 0.4	2.4	1, 1
HW 86	-0.75 ± 0.4	1.6	1, 1
L 4	-0.9 ± 0.2	3.1	1, 1
L 5	-1.2 ± 0.2	4.1	1, 1
L 6	-0.9 ± 0.2	3.3	1, 1
L 7	-0.6 ± 0.2	2.0	1, 1
	$Z/Z_{\odot} = -1.1 \pm 0.2$...	2, ...
L 17	...	1.26	..., 4
L 19	-0.75 ± 0.2	2.1	1,1
L 27	-1.3 ± 0.3	2.1	1,1
L 72	...	0.025 ± 0.010	..., 5
L 106	...	$0.89^{+0.23}_{-0.10}$..., 6
L 108	...	$0.89^{+0.37}_{-0.18}$..., 6
L 110	-1.15 ± 0.25	6.4 ± 1.1	3, 3
L 111	$Z/Z_{\odot} = -0.6 \pm 0.25$	$1.00^{+0.26}_{-0.21}$	2, 6

References. — (1) Piatti et al. 2005a; (2) Bica et al. 1986;
(3) Piatti et al. 2007b; (4) Rafelski & Zaritsky 2005; (5)
Piatti et al. 2007a; (6) Piatti et al. 2007c.

Table 5. Additional Cluster Samples

Cluster	Metallicity (dex)	Age (Gyr)	Reference Met., Age
L 11	-0.75 ± 0.13	3.5 ± 1.0	1, 1
L 113	-1.12 ± 0.12	6.0 ± 1.0	1, 1
NGC 121	-1.19 ± 0.12	10.5 ± 0.5	1, 2
L 1	-0.99 ± 0.11	7.5 ± 0.5	1, 2
K 3	-0.96 ± 0.12	6.5 ± 0.5	1, 2
NGC 339	-1.12 ± 0.10	6.0 ± 0.5	1, 2
NGC 416	-1.00 ± 0.13	6.0 ± 0.8	2, 2
L 38	-1.59 ± 0.10	6.5 ± 0.5	2, 2
NGC 419	-0.67 ± 0.12	1.4	2, 2
NGC 330	-0.94 ± 0.02	0.03	3, 4

References. — (1) Da Costa & Hatzidimitriou
1998; (2) Glatt et al. 2008b; (3)
Gonzalez & Wallerstein 1999; (4) WEBDA